The hyccin-containing protein ECDR1 interacts with PI3K1 and PI4K1 and regulates broad-spectrum disease resistance in rice

Shuang Zhang[1,2#], Lingzhi Meng[1,#], Zhichao Zhao[1,#], Changyan Qi[1], Chen Xie[1], Xiaokang Jiang[2], Ling Jiang[2], Yulong Ren[1], Zhijun Cheng[1], Jie Wang[1], Qibing Lin[1], Xiuping Guo[1], Xin Wang[1], Shanshan Zhu[1*], Cailin Lei[1*], Jianmin Wan[1,2*]

1 State Key Laboratory of Crop Gene Resources and Breeding, National Key Facility for Crop Gene Resources and Genetic Improvement, Institute of Crop Sciences, Chinese Academy of Agricultural Sciences, Beijing 100081, China

2 State Key Laboratory for Crop Genetics & Germplasm Enhancement and Utilization, Zhongshan Biological Breeding Laboratory, National Observation and Research Station of Rice Germplasm Resources, Nanjing Agricultural University, Nanjing 210095, China

# These authors contributed equally to this work.

*Correspondence: wanjianmin@caas.cn (J. Wan), leicailin@caas.cn (C. Lei), zhushanshan@caas.cn (S. Zhu).

The author responsible for distribution of materials integral to the findings presented in this article in accordance with the policy described in the Instructions for Authors (https://academic.oup.com/plphys/pages/General-Instructions) is Shanshan Zhu or Cailin Lei or Jianmin Wan.

Running head: ECDR1 regulating cell death and disease resistance in rice

Abstract

Programmed cell death and immunity in plants are finely orchestrated to promote antimicrobial defense while preventing autoimmunity. However, the molecular mechanisms involved are not fully understood. Here, we isolated a rice mutant *ecdr1* (*enhanced cell death and resistance 1*) that displayed an autoimmunity phenotype and enhanced resistance to rice blast and bacterial blight, and identified ECDR1 as a new shared component in PI3K and PI4K complexes, linking the hyccin-containing protein with plant defense responses. *ECDR1* was expressed at all developmental stages and in all tissues examined. The ECDR1 was highly conserved in function across monocots and dicots. The 113 bp deletion in the *ECDR1* promoter reduced its expression, leading to cell death and enhanced disease resistance. The ECDR1 was localized in plasma membrane, and interacted with TPR1 and TPR2 which in turn interacted with both PI4K1 and PI3K1, suggesting that ECDR1 could function as a component associated with not only PI4K complexes but also PI3K complexes to help catalyze PI into PI3P and PI4P. The lethality of all homozygous *ecdr1*, *pi3k1* and *tpr1 tpr2* mutants indicated the crucial roles of these genes in plant normal growth, which restricted our understanding of PI3K and PI4K functions. Alternatively, exogenous application of PI3K and PI4K inhibitors could substantially exacerbate the cell death and enhance disease resistance, implying their roles in plant immunity. Our findings provide novel insights into the regulatory mechanisms of ECDR1 in cell death and defense pathways, will aid in understanding the functions of PI3K and PI4K in plant immunity.

Key words: *ECDR1*, rice, disease resistance, phosphatidylinositol 3-kinase (PI3K), phosphatidylinositol 4-kinase (PI4K)

Introduction

Plants have developed a two-layered innate immunity mechanism to cope with pathogen attack: pathogen-associated molecular pattern (PAMP)-triggered immunity (PTI) conferred by pattern recognition receptors (PRRs) and effector-triggered immunity (ETI) conferred by

race-specific resistance (R) proteins (You et al. 2016; Gao et al. 2021). One common hallmark of both PTI and ETI is the hypersensitive responses (HR), one type of programmed cell death (PCD) at the infection sites, which not only acts to block biotrophic pathogen colonization but also have crucial role in activating systemic acquired resistance responses in plants (Shine et al. 2019; Pitsili et al. 2020; Zhang and Dong 2022). HR cell death can also occur as the result of autoimmune responses owing to the ectopic activation of immune-modulators, and thus plant immune machineries should be strictly controlled by negative regulators to avoid the runaway defense activation (Chakraborty et al. 2018; Pitsili et al. 2020; Zhang and Dong 2022). As an ideal means to characterize HR cell death, many plant lesion mimic mutants (LMM), showing autoimmunity phenotypes independent of pathogen infection, and their casual genes have been characterized, highlighting the importance of some cellular compartments and metabolic pathways in HR signaling (Bruggeman et al. 2015; Pitsili et al. 2020; Chen et al. 2025). Although HR cell death plays a crucial role in plant disease resistance, its underlying regulatory mechanisms are still not fully understood (You et al. 2016; Pitsili et al. 2020; Zhang and Dong 2022).

The phosphatidylinositol (PI or PtdIns) signaling pathway is a crucial regulator of biological function in eukaryotes. Phosphatidylinositol phosphates (also known as phosphoinositides) have long been recognized as major components of eukaryotic membranes essential for many functions, including cell signaling, membrane dynamics, and trafficking (Ischebeck et al. 2010; Zhao and Xue 2020). Phosphatidylinositol 4-kinase (PI4K) and Phosphatidylinositol 3-kinase (PI3K) phosphorylate PIs to produce phosphatidylinositol 4-phosphate (PI4P) and phosphatidylinositol 3-phosphate (PI3P), respectively, which act as common precursors for various phosphatidylinositol phosphates (Leprince et al. 2014; Pemberton et al. 2020). In Arabidopsis, twelve putative PI4Ks have been identified, among which eight belong to type II (AtPI4Kγ1–AtPI4Kγ8), and four belong to type III (AtPI4Kα1, AtPI4Kα2, AtPI4Kβ1 and AtPI4Kβ2) (Akhter et al. 2016). The actual identity of type II PI4Ks is questioned due to that they act as protein kinases and not lipid kinases; moreover, *AtPI4Kα2* is a pseudogene and homozygous *atpi4kα1* mutants are lethal, which restrict our understanding to PI4K functioning (Noack et al. 2022;

Starodubtseva et al. 2022). The *atpi4kβ1 atpi4kβ2* double mutants displayed mild growth defects including a stunted rosette, root length and cell elongation, linking an altered PI4K activity to actin filament disorganization, changes in vesicle trafficking and altered auxin response (Sašek et al. 2014; Starodubtseva et al. 2022). AtPI4Kα1 was considered to be a prime candidate for producing PI4P at the plasma membrane due to its localization at the plasma membrane and its catalytic activity validated *in vitro* (Stevenson-Paulik et al. 2003; Okazaki et al. 2015;). Noack et al. (2022) established that AtPI4Kα1 belongs to a 4-subunit complex composed of proteins from the NO-POLLEN-GERMINATION (NPG), EFR3-OF-PLANTS (EFOP), and HYCCIN-CONTAINING (HYC) families, and loss-of-function of any subunits leads to pollen lethality. The Arabidopsis HYC2, one human FAM126A (Family With Sequence Similarity 126) ortholog, is present in complex with PI4Kα1 and NPG2 in the sporophyte (Noack et al. 2022; Hsu et al. 2025). The lethality of *HYC2* loss-of-function indicates the indispensability of HYC2, and also poses obstacles for further investigating the roles of hyccin-containing proteins in plants. Moreover, both PI4K and PI4P have not been reported to be involved in host-pathogen interactions, and the roles of the PI4K subunits in plant immunity are still elusive.

Different from animals which have three types of PI3Ks, plants and yeasts possess only the type III PI3K, i.e. VPS34, which is encoded by a single-copy gene, *Vacuolar Protein Sorting 34* (*VPS34*) (Vanhaesebroeck et al. 1997; Liu et al. 2020). In Arabidopsis, VPS34 is part of a heteromeric PI3K (VPS34) complex with the kinase VPS15 and the protein AUTOPHAGY-RELATED 6 (ATG6). ATG6 can further recruit ATG14 or VPS38 as the fourth subunit, uniquely generating complex I or complex II isoforms, which act in the autophagy and endocytosis, respectively (Ohashi et al. 2019; Bhati et al. 2021; Liu et al. 2020). So far, understanding of the PI3K complexes is limited owing to the infertility of plants missing any core subunits, VPS34, VPS15 and ATG6 (Lee et al. 2018; Liu et al. 2018, 2020). Homozygous *vps38*, *atg14a atg14b*, or *atg14a atg14b vps38* mutants were viable and fertile even though their growth and development were substantially affected, which provided a venue to study PI3K and PI3P functions in Arabidopsis (Lee et al. 2018; Liu et al. 2020). The plant PI3Ks and PI3Ps have been shown to involve in diverse plant physiological processes, including pollen

development, root hair growth, stomata closure, and proline catabolism (Leprince et al. 2014; Liu et al. 2020), however, their roles in plant immunity are little known. Moreover, although RBL1, a CDP-DAG synthase that synthesizes cytidine diphosphate diacylglycerol (CDP-DAG), a PI precursor, was reported to be associated with an autoimmunity phenotype in the LMM *rbl1* (Sha et al. 2023), the connection of PI signaling pathways with plant defense responses is still hardly understood.

Here, we isolated a rice mutant *ecdr1* (*enhance cell death and resistance 1*), which exhibited an autoimmunity phenotype and enhanced broad-spectrum resistance to blast caused by *Magnaporthe oryzae* (*M. oryzae*) and bacterial blight caused *Xanthomonas oryzae* pv. *oryzae* (*Xoo*). *ECDR1* encoded a hyccin-containing protein which was highly conserved across monocots and dicots, and was expressed at all developmental stages and in all examined tissues. The *ECDR1* gene negatively regulated cell death and defense responses in rice. The ECDR1 protein was localized in plasma membrane, and directly interacted with TPR1 and TPR2 which in turn interacted with both PI4K1 and PI3K1 (VPS34), suggesting that ECDR1 could function as a component associated with not only PI4K complexes but also PI3K complexes to help catalyze PI into PI3P and PI4P. Furthermore, exogenous application of PI3K and PI4K inhibitors could exacerbate the phenotypes of cell death and enhance disease resistance in *ecdr1* and wild-type (WT) plants, also implying their roles signaling in plant immunity. These findings will aid in understanding of regulatory mechanisms of ECDR1, PI3K and PI4K in HR cell death and defense responses in plants.

Results

ecdr1 is an autoimmunity and broad-spectrum disease-resistance mutant

In order to identify genes that control autoimmunity phenotypes featured with PCD and enhanced disease resistance in rice, we screened a genetically stable LMM mutant *ecdr1* from an anther culture-derived M4 population (approximately 550 lines) of the cross 09-2131 × Kendao 2016 at the tillering stage (Supplemental Fig. 1). The *ecdr1* mutant began to show small, yellowish-brown lesions from top to bottom of the lower (older) leaves about 22 days after sowing (DAS) (Supplemental Fig. 2A), and such lesions increased in both

number and size at the early flowering stage, followed by rapid senescence of the whole plant at late flowering stage, while the WT (sib-line 1503089) plants stay green and normal (Supplemental Fig. 2). As a result, *ecdr1* displayed growth retardation with reduced plant height, fertility and grain yield (Supplemental Table S1).

ecdr1 exhibits a typical programmed cell death (PCD) phenotype, characterized by deep trypan blue staining, intense TUNEL-positive signals and H_2O_2 accumulation (Fig. 1, A to E). Antioxidant enzyme activities assays showed that the activities of catalase (CAT), peroxidase (POD), and superoxide dismutase (SOD) in *ecdr1* were 0.34-, 5.0-, and 1.35-fold of those in the WT plant (Supplemental Fig. S3), suggested that the *ecdr1* mutant may actively responded to the H_2O_2 accumulation and the decreased CAT activity was the main cause of $O_2^{\cdot-}$ excessive accumulation in *ecdr1* mutant. These results suggested the PCD phenotype of *ecdr1* was tightly associated with excessive ROS accumulation and irreversible membrane damage in cells.

Given that *ecdr1* showed a PCD phenotype associated with excessive ROS accumulation, it is speculated that the *ecdr1* mutation may lead to the activation of defense responses and enhance disease resistance. We thus examined the transcriptional levels of four defense-related marker genes *AOS2*, *PBZ1*, *PR1a* and *PR1b* (Fitzgerald et al. 2004; Wang et al. 2017) in *ecdr1* and WT. The expression levels of the four genes in the *ecdr1* plants at 14 DAS (before appearance of visible lesions in *ecdr1*) were almost same as those in WT plants, however, their expression in *ecdr1* at 28 DAS (lesions clearly visible in lower leaves of *ecdr1*) increased and was 76.49-, 17.31-, 60.80-, and 12.41-fold higher, respectively, than that in WT (Fig. 1F), indicating that defense responses involved with jasmonic acid (JA) biosynthetic and salicylic acid (SA) signaling pathways were activated with appearance of the PCD phenotype in *ecdr1*. To examine whether the *ecdr1* mutant gains disease resistance, we inoculated the *ecdr1* and WT seedlings at 28 DAS with the virulent *M. oryzae* isolates 99-26-2 and Zhong 10-8-14, and showed that both lesion lengths and fungal biomass in *ecdr1* were significantly decreased compared to in WT (Fig. 1, G to I). In another test, we inoculated the flag leaves of *ecdr1* and WT at the flowering stage with four *Xoo* isolates, P2, P6, C5 and T1 and showed that the lesion lengths were significantly

decreased in *ecdr1* relative to WT (Fig. 1, J and K). Together, all above-mentioned results indicated that *ecdr1* is an autoimmunity mutant with enhanced resistance to both fungal and bacterial diseases.

ECDR1* was responsible for the autoimmunity phenotype and enhanced disease resistance in *ecdr1

Genetic analysis revealed that the PCD phenotype of *ecdr1* was controlled by a single recessive nuclear gene (Supplemental Table S2). To isolate the *ECDR1* gene, a F_2 mapping population was developed by crossing *ecdr1* with *indica* variety CO39. The *ECDR1* locus was finely mapped to a 33.2 kb region on chromosome 11, which contains seven predicted open reading frames (ORFs) based on the rice genome annotation project database (https://rice.uga.edu/jb2/?session= local-FCWky9JwdGzmRw33L332K) (Fig. 2A). Sequence alignment of the target region identified only 546 bp deletion (from the 127th base upstream of start codon of *ORF4*) (*LOC_Os11g06860*) to the 18th base downstream of stop codon of *ORF5* (*LOC_Os11g06870*) in *ecdr1* compared to WT (Fig. 2B), and the expression levels of *ORF4* and *ORF5* in *ecdr1* were markedly decreased to 0.11- and 0.06-fold, respectively, of those in WT (Supplemental Fig. S4A). Therefore, we preferentially considered *ORF4* and *ORF5* to be candidates of *ECDR1*.

To demonstrate whether the 546 bp deletion was responsible for the *ecdr1* mutant phenotype, we carried out genetic complementation assays. Two plasmids containing the WT-derived genomic fragments of *ORF4* or *ORF5*, spanning the entire coding region, 2.5 kb upstream regulatory sequence and 1.5 kb downstream regulatory sequence (both harboring the 546 bp), were introduced into the calli of *ecdr1* mutants, respectively. All the positive *ORF4*-transgenic plants exhibited a complete rescue of both the PCD and growth phenotypes of *ecdr1* (Fig. 2C and Supplemental Fig. S5), whereas the positive *ORF5*-transgenic plants cannot (Supplemental Fig. S4B). We also generated *ORF4* overexpression transgenic plants by transforming the entire coding sequence of *ORF4* under the control of the maize ubiquitin promoter into *ecdr1* calli. We observed that all *ORF4* overexpressing lines can also rescue *ecdr1* phenotype (Supplemental Fig. S4C). Furthermore, we

inoculated the *ORF4*-complementation and *ORF4*-overexpression together with *ecdr1* and WT plants with *Xoo* strains, and observed that both of them displayed elevated susceptibility with lesion lengths significantly longer than the *ecdr1,* like the WT (Fig. 2, D and E; Supplemental Fig. S4, D to F). Therefore, we concluded that *ORF4* (*LOC_Os11g06860*) was the functional *ECDR1* gene, in which the 546 bp deletion is responsible for the autoimmunity phenotype featured with PCD and enhanced disease resistance in *ecdr1*.

A 113 bp in *ECDR1* promoter region was essential for PCD regulation in rice

Sequence analysis revealed that the 546 bp deletion in *ecdr1* consisted of a 433 bp transposon element named miniature *ping* (*mping*), which was classified as a *Tourist*-like miniature inverted-repeat transposable element (MITE) (Jiang and Wessler 2001; Naito et al. 2006), and its two flanking sequences, 99 bp and 14 bp (Fig. 2B and Supplemental Fig. S6). To understand the origin of the 546 bp deletion in *ecdr1*, we compared the promoter sequences of *ECDR1* in WT, *ecdr1* and the well-sequenced *japonica* Nipponbare (NIP) (http://plants.ensembl.org/Oryza_sativa/Info/Index) together with the three pedigree parents, ZH11, CY and KD2016 (Supplemental Fig. S1), and showed that the 433 bp (*mping*) insertion was only present in WT and KD2016, and the 113 bp deletion (99 bp + 14 bp) was only present in *ecdr1* (Fig. 2F and Supplemental Fig. S6). These results suggested that the 433 bp insertion in WT originated from cv. KD2016, and the 546 bp deletion in *ecdr1* could result from the activation and transposition of the *mping* transposon during the anther tissue culture (Supplemental Fig. S1).

To determine how the 546 bp deletion affected *ECDR1* transcription (Supplemental Fig. S4A), we test activities of the *ECDR1* promoter in WT (P^{WT}, 2.5 kb), WT promoter with a 433 bp (*mping*) deletion ($P^{WT\,\Delta\,433\,bp}$, 2 kb), *ecdr1* mutant (P^{ecdr1}, 1.9 kb minus the 546 bp) and the only 113 bp sequence (P^{113}, 546 bp minus the 433 bp of *mping*) by means of transient gene expression assays using a luciferase reporter (LUC). The results showed that the luciferase activity of P^{ecdr1} was significantly decreased to 0.20-fold of that of P^{WT}, whereas the luciferase activity of P^{113} kept an approximate level as that of P^{WT} (Fig. 2G), indicating the

113 bp is essential for *ECDR1* promoter activity, and its deletion can inhibit *ECDR1* promoter activity in *ecdr1*. To confirm this, we further detected expression of *ECDR1* in WT, *ecdr1* and NIP using qRT-PCR, and showed that the expression level of *ECDR1* in WT was similar to that in NIP, and at least 34.93-fold higher than that in *ecdr1* (Fig. 2H), which was consistent with the promoter activity levels of the P^{WT}, P^{ecdr1} and P^{113} constructs (Fig. 2G). These results indicated that it is the 113 bp deletion caused by the *mping* transposition that compromised the promoter activity and expression level of *ECDR1* in the *ecdr1* mutant, contributing to the PCD phenotype.

Expression profile of *ECDR1* and Subcellular localization of ECDR1

Quantitative real-time PCR (qRT-PCR) analysis showed that *ECDR1* was ubiquitously expressed in roots, stems, leaves, leaf sheaths, and panicles of both WT and *ecdr1* plants (Fig. 3A). To investigate whether the PCD phenotype and leaf age is related to the expression level of *ECDR1* in *ecdr1*, the expression level of *ECDR1* in different aged leaf blades at the five-leaf stage was checked. As a result, the *ECDR1* expression level was decreased with the increase of leaf ages in both *ecdr1* and WT plants, particularly in the lower (older) leaves of *ecdr1* (Fig. 3B), which was consistent with the increasingly severe PCD phenotype.

To determine the subcellular localization of ECDR1, we generated the ECDR1-GFP fusion vector through cloning the full-length CDS of *ECDR1* into the N-terminus of green fluorescent protein (GFP) from PAN580 vector, and then transformed it into rice protoplasts with plasma membrane marker secretory carrier-associated membrane protein 1 (SCAMP1)-mCherry. As a result, strong yellow signals which overlapped the GFP and red fluorescent signals was observed in the plasma membrane (Fig. 3C), suggesting that ECDR1 was a plasma membrane-located protein.

The ECDR1 protein was highly conserved in function across monocots and dicots

Sequence analysis showed that ECDR1 was a hyccin-containing protein, consisting of 428 amino acids. A BLAST search revealed that ECDR1 shared high sequence identity with some monocot plants such as *Brachypodium distachyon* (79.3%), *Zea mays* (85.7%),

Setaria italica (86.6%), *Sorghum bicolor* (86.1%), and relative lower identify with dicot plants like *Glycine max* (44.6%), *Arabidopsis thaliana* (HYC2 42.41%) (Fig. 4A to B). Phylogenetic analysis showed that homologs of ECDR1 were clearly separated into two clusters monocots and dicots, and ECDR1 was closest to *Brachypodium distachyon* (*BRADI_4g24260v3*) (Fig. 3D).

To investigate the function of the hyccin domain in ECDR1, we conducted complementation test by transforming the truncated sequences of *ECDR1* including 1-600 bp (ECDR1$^{1\text{-}200}$), 601-1284 (ECDR1$^{201\text{-}428}$), 1-900 bp (ECDR1$^{1\text{-}300}$), 301-1284 bp (ECDR1$^{101\text{-}428}$), 174-1233 bp (ECDR1^{hyccin}) sequences under control of the ubiquitin promoter. The mutant phenotype was completely rescued in the ECDR1^{hyccin} positive plants, whereas the other vectors failed (Fig. 4C). These results showed that the function of *ECDR1* depended on the hyccin domain. To examined whether the function of *ECDR1* was conserved among species, the coding regions of *ECDR1* homologs from monocots *Zea mays*, *Setaria italica*, and dicots *Glycine max*, *Arabidopsis thaliana* were overexpressed in *ecdr1*. As a result, all resulting transgenic positive plants rescued the *ecdr1* mutant phenotype (Fig. 4D), suggesting that *ECDR1* was highly conserved in function among plants.

ECDR1 could physically interact with PI4K1 and TPR1/2

The hyccin-containing protein FAM126A is a part of a PI4KIIIα complex, in which TTC7 (Tetratricopeptide Repeat Protein 7) bridges PI4KIIIα and FAM126 together to form the complete PI4KIIIα enzyme to catalyze PI into PI4P in human (Baskin et al. 2016; Dornan et al. 2018; Lee et al. 2018). To determine whether there exists the similar PI4K complex in rice, we firstly used the PI4KIIIα and TTC7 amino acid sequences from human genome as queries to blast in the Gramene database (http://ensembl.gramene.org/Tools/Blast?db=core). As a result, 3 and 5 homologs were identified for PI4KIIIα and TTC7 in rice, respectively (Supplemental Table S4). The three rice PI4KIIIα homologs could be classified into two types, PI3K and PI4K, based on the sequence annotation in NCBI, in which PI3K1 and PI3K2 belonged to PI3K type, and PI4K1 belonged to PI4K type (Supplemental Table S4, Supplemental Fig. S8). The five rice TTC7

homologs were name as TPR1 to TPR5 for easy description due to their common tetratricopeptide repeat (TPR) domains (Supplemental Table S4, Supplemental Fig. S9, Supplemental Fig. S10). Secondly, we conducted the yeast two-hybrid (Y2H) assays, and showed that ECDR1 interacted with both TPR1 and TPR2, and both TPR1 and TPR2 in turns interacted with PI4K1 (Fig. 5A). To further verify these interactions, we performed the firefly luciferase complementation imaging (LCI) and co-immunoprecipitation (Co-IP) assays. As a result, strong fluorescence signals were detected in the combinations of both ECDR1 and PI4K1 with TPR1/2 (TPR1 and TPR2) in *Nicotiana benthamiana* leaves via the LCI assay (Fig. 5B); and both Flag-ECDR1 and Flag-PI4K1 were co-immunoprecipitated by TPR1/2-GFP in total leaf extract of *N. benthamiana* in the Co-IP assay (Fig. 5, C and D). To determine the region of ECDR1 for its interaction with TPR1/2, we constructed a deletion series of ECDR1 based on domain prediction (Fig. 4B), and identified the hyccin domain of ECDR1 to be indispensable for the ECDR1-TPR12 interaction (Fig. 5F). These results validated that TPR1/2 could indeed bridge together PI4K1 and ECDR1, and thus we could deduce that ECDR1 was a part of the rice PI4K1 complex in the same manner as its human homolog FAM126A.

ECDR1 could be a novel component of the PI3K1 complex

Since two rice homologs of human PI4KIIIα, PI3K1 and PI3K2, were classified into the PI3K type (Supplemental Table S4, Supplemental Fig. S8B), we speculate that ECDR1 and its bridge protein TPR1/2 could also act in PI3K complexes in rice. Thus, we firstly performed blast searches of rice genome database using the protein sequences of all Arabidopsis complex components, including VPS34, VPS15, ATG6, ATG14 and VPS38 as queries, and found that these subunits shared 59.60-70.87%, 49.81%, 45.16-53.24%, 46.23% and 38.40% amino acid identities with their counterparts PI3K1-PI3K2, VPS15, ATG6A-ATG6C, ATG14 and VPS38 in rice, respectively (Supplemental Table S6). PI3K1 shared much higher identity with VPS34 (70.87%) than did PI3K2 (58.87%) (Supplemental Fig. S8B), and thus probably represented the PI3K (VPS34) in rice. Secondly, we performed Y2H, LCI and Co-IP assays of ECDR1 and TPR1/2 with these subunits, and showed that TPR1/2 interacted with PI3K1, and both ECDR1 and TPR1/2 interacted with ATG6A and ATG6B (ATG6A/B) (Fig. 5, A,

B and E; Fig. 6A and B). The results suggested that ECDR1 could be a novel component of the PI3K1 complex, in which TPR1/2 bridged together ECDR1 and PI3K1, and both ECDR1 and TPR1/2 directly interacted with ATG6A/B.

ECDR1, *TPR1/2*, *PI4K1*, and *PI3K1* were essential for rice normal growth

To investigate the biological significance of *ECDR1*, *TPR1/2*, *PI4K1* and *PI3K1* in rice, we knocked out these genes using CRISPR/Cas9 technology in WT plants. The *ecdr1-3*, *ecdr1-4*, *pi3k1-3*, and *pi3k1-4* mutant plants, each carrying 1 bp insertion or 13 bp deletion leading to a frameshift mutation and loss-of-function (Fig. 6, C and D), all could not generate homozygous null mutants in either T_0 or T_1 generations, indicating the homozygous lethality of *ecdr1* or *pi3k1*. In the TPR1/TPR2 knockout lines, we obtained three *tpr1* (*tpr1-1*, *tpr1-2* and *tpr1-3*) and two *tpr2* (*tpr2-1*, *tpr2-2*) homozygous null mutants, respectively, all of which caused open reading frame shift (Fig. 6, E and F), but displayed no obviously phenotype variations compared to the WT plants (Supplemental Fig. S11). We speculated that *TPR1* and *TPR2* may have redundant role in rice due to their 42.76% protein identity. Thus, we constructed the double mutants of *TPR1* and *TPR2* using CRISPR/Cas9 technology, and found that *tpr1 tpr2* null mutants were also lethal. Furthermore, the complete loss-of-functions of *PI4Kα1* homologs in yeast, mice, and Arabidopsis also caused lethality (Batrouni et al. 2022; Noack et al. 2022). These results indicated that *ECDR1*, *TPR1/2*, *PI4K1*, and *PI3K1* were essential for plant normal growth, and that null mutations of these genes may activate more excessive autoimmunity phenotypes than the promoter mutation of *ECDR1* in *ecdr1* (Fig. 1, A to E), leading to their lethality.

The activity inhibition of PI3K1 and PI4K1 could trigger cell death and immunity in rice

Given that ECDR1 could be a component associated with the PI3K1 and PI4K1 complexes, we envisioned that the cell death and immunity in *ecdr1* plants may also be associated with the activity inhibition of PI3K1 and PI4K1. To test this hypothesis, we sprayed 25-day-old *ecdr1* mutant seedlings with wortmannin (Wort), a well-characterized inhibitors of PI3K (VPS34) and PI4K (Etkovitz et al. 2007; Fujimoto et al. 2015), and found that numerous visible lesions appeared on the third and fourth leaf blades of the treated plants while few

lesions on the leaf blades of the control plants on the 2nd and 6th day after the treatment (Fig. 7A, B). Trypan blue staining showed that the treated leaf blades exhibited much more and deeper blue spots compared to the control, confirming the aggravated cell death in *ecdr1* (Fig. 7C). Furthermore, we separately and jointly treated *ecdr1* seedlings using the PI3K-specific inhibitor, LY294002, and the PI4K-specific inhibitor, PAO. As a result, compared with the dimethyl sulfoxide (DMSO) treatment as the control, the combined treatment with both inhibitors substantially aggravated the cell death phenotype, whereas separate treatment with either LY294002 or PAO had no such effect (Fig. 7D). These results indicate that the cell death phenotype in *ecdr1* could be associated with the activity inhibition of both PI3K1 and PI4K1 in rice. Meanwhile, we measured the PI3P and PI4P levels in the *ecdr1* and WT leaves, and showed that those in *ecdr1* were significantly decreased relative to WT (Fig. 7E, F), suggesting the crucial roles of ECDR1 in PI3P and PI4P regulation.

To determine the association of PI3K1 and PI4K1 activities with immunity, we firstly sprayed the WT seedlings with wortmannin, and found that this treatment could also induce severe cell death (Fig. 7G). Secondly, we inoculated the wortmannin-treated leaves with *Magnaporthe oryzae* isolate Zhong10-8-14, and found that the treatment could indeed markedly enhance disease resistance relative to the control (Fig. 7, H to J), suggesting the actual association of the PI3K1 and PI4K1 activity inhibition and the enhanced disease resistance in rice.

Transcriptome sequencing suggested that *ecdr1* involved in multiple defense pathways

To understand the defense mechanism in the *ecdr1* mutant, we performed transcriptome sequencing of both the WT and *ecdr1* mutant at 14 DAS (before appearance of visible lesions in *ecdr1*) and 28 DAS (lesions clearly visible in lower leaves of *ecdr1*). In total, 128 differentially expressed genes (DEGs, 31 up-regulation and 97 down-regulation) at 14 DAS, and 7723 DEGs (3245 up-regulation and 4478 down-regulation) at 28 DAS were identified with > two-fold changes, respectively, suggesting a large effect of the *ECDR1* mutation on plant growth after the appearance of lesion mimics in *ecdr1*.

KEGG enrichment analysis showed that 31 significantly up-regulated DEGs and 10 down-regulated DEGs involved in plant-pathogen interaction were detected in *ecdr1* relative to WT at 28 DAS (Supplemental Fig. S13, Supplemental Table S7). They were involved in mitogen-activated protein kinases (MAPKs) signaling cascade including *RLCK278*, *MAPK4*, *MAPK3*, *WRKY53*; transcription regulation including *WRKY13/31/47/71/89*; calcium signaling including seven *CaMs* and five CDPKs; pathogen-associated molecular patterns recognition including two pattern recognition receptor (PRR) *SDS2* and *CEBiP*; ROS production including four NADPH oxidases *RBoHs*; recognition of avirulence effectors including two nucleotide binding site and leucine-rich repeats protein (NBS-LRR) *RPM1* and *RPS2* and two resistance protein *HSP90* and *SGT1* (Supplemental Fig. S13). 22 significantly up-regulated genes involved in JA biosynthesis were also identified, including three *LOXs*, three *AOSs* and two *ACXs*, two ethylene (ETH) biosynthesis-related genes (*ACS2* and two *ACOs*), and ten SA biosynthesis and signaling-related genes (two *PALs, NPR1*, three *TGAs*, *WRKY67*, *BIERF3*, *PR1a* and *PR1b*) (Supplemental Fig. S13, Supplemental Table S8). These results indicated the decreased expression of *ECDR1* leads to activation of innate immunity, including activation of both PTI and ETI, induction of anti-microbial proteins and accumulation of phytoalexins, and so on, thus resulting in broad-spectrum resistance of *ecdr1* to fungal and bacterial pathogens.

Multiple *ECDR1* haplotypes are biological relevant to some important traits

Given that the 113 bp deletion is unique to the *ecdr1* mutant (Fig. 2F and Supplemental Fig. S6), to strengthen the biological relevance and potential agronomic importance of *ECDR1*, we performed a systematic haplotype analysis of the *ECDR1* promoter region in the 3K rice accessions (https://snp-seek.irri.org/). As a result, six SNPs were identified in the promoter regions, and five haplotypes were defined (Supplemental Figure S7A). Haplotype 1 (Hap1) was predominant in *Xian/indica* (87.1%), *aus* (5.8%) and tropic *Geng/japonica* (3.7%), and tightly associated with grain length and grain length-width ratio; Hap2 was predominant in *Geng/japonica* (88.2%) and tightly associated with grain width and thousand-grain-weight; and Hap4 was predominant in *Aus* (61.2%) and *Xian/indica* (26.4%), and tightly associated with panicle number and culm number. The results indicated that these haplotypes had significant biological relevance and potential

agronomic importance of *ECDR1* (Supplemental Figure S7B to J), probably providing useful allelic diversity for rice improvement.

Discussion

ECDR1 encodes a highly conserved hyccin protein that negatively regulates cell death and immunity

Plant responses to pathogen invasion are usually accompanied by rapid cell death around the infection sites, a reaction known as HR, which inhibits further growth and spread of pathogens (Lam et al. 2001; Van Durme and Nowack 2016). In this study, we characterize a novel enhanced cell death and resistance mutant named as *ecdr1* (Fig. 1 and Supplemental Fig. S2). The map-based cloning and transgenic assays revealed a 113 bp deletion in *ECDR1* promoter region affected the promoter activity and expression level of this gene, which was responsible for mutant phenotypes in *ecdr1* (Fig. 2). Although we had annotated the potential cis-regulatory elements within this 113 bp region (Supplemental Table S3), whether and how these elements affect the functioning of this region need to be investigated.

Amino acids sequence analysis revealed ECDR1 is a function-unknown protein, encompassing the only recognizable domain designated as hyccin (Fig. 4B). Overexpression and protein-protein interaction assays of truncated *ECDR1* addressed that the hyccin domain determined the ECDR1 protein function (Fig. 4 and Fig. 5F). ECDR1 were highly conserved among different plants evidenced as follows: (1) ECDR1 shared relative high identities with other plants including both monocots and dicots (Fig. 3D); (2) the cell death phenotype in *ecdr1* could be rescued by introduction of the *ECDR1* homologs from *Zea mays*, *Setaria italica*, *Glycine max* and *Arabidopsis thaliana* (Fig. 4D).

We showed that ECDR1 negatively regulated cell death, which was indicated by that the deeper trypan blue staining, more accumulation of H_2O_2, $O_2^{\cdot-}$ and more intense TUNEL-positive signals in *ecdr1* relative to WT (Fig. 1, A to E). We also found that the immunity was activated in *ecdr1*, which was confirmed by enhanced resistance to blast and bacterial blight and increased expression of defense-related genes in *ecdr1* relative to WT (Fig. 1, F

to K). KEGG enrichment analysis of DEGs between *ecdr1* and WT based on transcriptomic data revealed that a number of defense-related genes were significantly up-regulated in *ecdr1*, including those PTI-related *SDS*, *CEBiP*, *MAPKs*, *RBoHs*, *CDPKs*, *CaMs*, RLCK278, MAPK4, MAPK3 and WRKY53, ETI-related *RPM1*, *RPS2*, *HSP90*, *SGT1*, *PR1a/b* and *WRKY13/31/47/71/89*, and SA, JA and ETH biosynthesis/signaling-related *LOXs*, *AOSs*, *ACXs*, *PALs*, *ACS2*, *ACOs*, *NPR1*, *TGAs*, *BIERF3* and *WRKY67* (Supplemental Fig. S13). These results suggested that the decreased expression of *ECDR1* caused by the 113 bp deletion of its promoter region leads to activation of innate immunity, thus resulting in broad-spectrum resistance of *ecdr1* to fungal and bacterial pathogens.

ECDR1 could act as a new component in rice PI4K1 and PI3K1 complexes

In human, the ECDR1 homolog FAM126A could form a PI4KIIIα complex with TTC7, EFR3 and PI4KIIIα. In this complex, both PI4KIIIα and TTC7 regulated PI4P biosynthesis by impacting the activity of the PI4KIIIα complex (Baskin et al. 2016; Lees et al. 2017; Dornan et al. 2018). All the homologs of PI4KIIIα complex were identified in rice (Supplemental Table S4), i.e. PI4K1, ECDR1, and TPR1 and TPR2, which shared low identity with their human counterparts (Supplemental Table S4), but much higher identity with their Arabidopsis counterparts, i.e. PI4Kα1 (62.86%), HYC2 (42.41%), and NPGR2 (51.87% and 40.45%), respectively (Noack et al. 2022). ECDR interacts with TPR1 and TPR2 which both in turn interacts with PI4K1 in rice in similar manners as did FAM126A and HYC2, and *HYC2* can rescue the *ecdr1* phenotypes (Fig. 4C), suggesting the functional conservation between ECDR1 and its homologous proteins in PI4K complexes. The human and Arabidopsis PI4K complexes both contain an additional subunit, EFR3 or EFOP, which recruits the complex to the plasma membrane (Baskin et al. 2016; Dornan et al. 2018; Noack et al. 2022; Hsu et al. 2025). We identified a total of four rice EFR3 homologs named as EFR3-1 to EFR3-4, but did not detect interactions of these EFRs with TPRs in rice using Y2H system. We postulate possible explanations for this inconsistency as follows: (1) the function of EFR3 is substituted by other proteins in rice; (2) the PI4KIIIα complexes are only partially conserved among rice, human and Arabidopsis.

We have shown that ECDR1 interacts not only with PI4K1 but also with PI3K1 (VPS34) in rice (Fig. 5). In mammal, yeast and *Arabidopsis*, VPS34 forms the PI3K complex with other two core subunits VPS15 and ATG6, and the fourth subunit, ATG14 or VPS38, further discriminates the complex to complex I or complex II (Funderburk et al. 2010; Liu et al. 2020). In the present study, we identified the rice counterparts of ATG6, VPS34, VPS15, ATG14, and VPS38 (Supplemental Table S5), and confirmed that the two types of complexes also existed in rice by interactions between VPS15 and VPS34, ATG6 or VPS38, between ATG6 and VPS38 or ATG14 in standard Y2H and split-ubiquitin Y2H assays (Supplemental Fig. S12). We also found that all ECDR1, TPR1 and TPR2 interacted with ATG6 by standard Y2H and BiFC assays (Fig. 6, A to B). These results suggested that ECDR1 could function as an essential component not only in PI4K complexes but also in PI3K complexes. Since all homozygous knockout mutants of *PI3K*, *TPR1/2*, and *ECDR1* were lethal, we once attempted to construct their knockdown mutants using the RNAi technique, but failed to get survival plants either. We speculated that the expression level of these genes was also crucial for their function. Considering lethality of homozygous null mutants of all main components in plant PI3K and PI4K complexes, including NPG1, PI4Kα1, EFOPs, VPS34, VPS15 and ATG6 (Harrison-Lowe and Olsen 2008; Lee, Bak, et al. 2008; Lee, Kim, et al. 2008; Noack et al. 2022; Xu et al. 2011), the availability of *ecdr1* mutants, in which *ECDR1* expression was decreased due to a 113 bp deletion in its promoter region, will provide a venue to study PI4K1 and PI3K1 functions throughout the rice life cycle.

ECDR1 could regulate cell death and disease resistance through impacting the PI3K1 and PI4K1 activities

Given the role of ECDR1 in the formation of both PI3K1 (VPS34) and PI4K1 (PI4KIIIα1) complexes, we hypothesized that it modulates their kinase activities and consequently the levels of PI3P and PI4P. To test this, we exogenously applied the broad-spectrum inhibitor Wort (targeting both PI3K and PI4K), the PI3K-specific inhibitor LY294002, and the PI4K-specific inhibitor PAO to both WT and *ecdr1* seedlings. The Wort treatment could significantly promote and aggravate cell death occurrence in *ecdr1*, whereas both

LY294002 and PAO treatments alone did not cause any obvious phenotypic changes (Fig. 7, A to C). However, the joint application of LY294002 and PAO inhibitors could significantly promote and aggravate the cell death phenotype in both *ecdr1* seedlings (Fig. 7D). Furthermore, the exogenous application of Wort on WT seedlings could also activate the cell death and enhance disease resistance in WT (Fig. 7, G to J). These results suggested that the simultaneous inhibition of PI3K1 and PI4K1 activities could be responsible for the autoimmunity phenotype in *ecdr1,* the reason for which is worthy of careful consideration. The quantification of phosphatidylinositol phosphates confirmed that *ecdr1* leaves accumulated markedly lower levels of both PI3P and PI4P compared with WT (Fig. 7, E and F), indicting the regulation of ECDR1 for PI3P and PI4P. In addition, the RNA-seq analysis showed that multiple defense-related genes were extensively upregulated in *ecdr1* relative to WT (Supplemental Fig. S13, Supplemental Table S8), indicating the roles of ECDR1 in innate immunity regulatory. Recent studies showed that PI4P regulates vesicle trafficking critical for PRR localization, and impaired PRR localization may disrupt immune homeostasis (Fang et al. 2023; Zheng et al. 2023); and PI3P is essential for autophagy and endocytosis, and reduced PI3P levels may also affect the degradation of intracellular immune signaling components (Gui et al. 2019; Zhang et al. 2020; Steinfeld et al. 2021). In mammals, both PI3P and PI4P play roles in the cGAS-STING pathway, decreased levels of which could affect function of lipid metabolism-or trafficking-related proteins, leading to various autoimmune diseases (Gui et al. 2019; Zhang et al. 2020; Fang et al. 2023). In this study, we validated the association of the inhibited PI3K and PI4K activities and reduced PI3P and PI4P levels with the autoimmunity phenotypes and enhanced disease resistance in *ecdr1*. Thus, we could deduce that the reduced PI3P and PI4P levels might disrupt function of lipid metabolism-or trafficking-related proteins, leading to disturbed lipid homeostasis, extensive upregulation of defense-related genes and the subsequent development of the autoimmunity phenotypes and defense responses in *ecdr1*.

Taken together, we could conclude that the mutation of ECDR1 suppressed PI3K1 and PI4K1 activities, which caused decreased PI3P and PI4P levels, ultimately leading to the cell death and enhanced disease resistance in *ecdr1* (Fig. 8). To our knowledge, this is the

first report that a hyccin-containing protein is involved in cell death and the defense response in plants, and that ECDR1 acts as a shared component associated with rice PI3K1 and PI4K1 complexes. However, the mechanisms of the kinase regulation by ECDR1 have not been touched upon in the present study. To comprehensively elucidate the regulatory mechanism of *ECDR1* in prevention of autoimmunity, further analyses of ECDR1, PI3K1 and PI4K1 for their function in the PI signaling pathway need to be undertaken. Understanding the relationships between ECDR1-mediated PI signaling and cell death, in connection with defense response will be part of that effort.

Methods

Plant materials and growth conditions

The *ecdr1* mutant (line # 1503090 with homozygous lesion mimic phenotype) was originally identified from the anther culture-derived M_4 population of a cross between *japonica* cultivar Kendao 2016 and *japonica* line 09-2131, a F_5 line derived from a cross between *japonica* cultivar Zhonghua11 and *japonica* cultivar Chunyang (Supplemental Fig. S1). Reciprocal crosses were made between *ecdr1* and WT (sib-line # 1503089 with homozygous normal phenotype), and their F_1 and F_2 progenies were used as for genetic analysis. The F_2 population derived from a cross of *ecdr1* and *indica* cv. CO39 was used for map-based mapping. All plants, except specified, were grown in a paddy field at the Shunyi Experimental Station, Institute of Crop Sciences in Beijing during May-October, the normal rice-growing season.

Histochemical assay

Leaves of *ecdr1* and WT at 28 DAS were harvested for histochemical assays. Trypan blue staining for dead cells was performed as described previously (Qiao et al. 2010). In brief, samples were submerged in a 70°C trypan blue solution (2.5 mg/mL trypan blue, 25% (W/V) lactic acid, 23% water-saturated phenol and 25% glycerol in H_2O), infiltrated for 10 min, and then heated over boiling water for 2 min and left to stain overnight. After de-staining in chloral hydrate solution (25 g in 10 mL of H_2O) for three days, samples were equilibrated with 70% glycerol for microscopy analysis.

DAB staining for H_2O_2 accumulation and NBT staining for $O_2^{\cdot-}$ accumulations were performed as described previously (Qiao et al. 2010). In brief, samples were transferred in DAB staining solution (1% 3, 3'-diaminobenzidine, pH = 5.7) and NBT staining solution (0.05% nitro blue tetrazolium in 50 mM sodium phosphate buffer), respectively, and centrifuged until completely immersed in the buffer. After 12 h inoculation in a vacuum, the samples were decolorized with 90% ethanol.

The ROS and MDA contents, and CAT, POD and SOD activities were measured using test kits according to manufacturer's instructions (Jiancheng, Nanjing). For TUNEL assay, the 28-day-old leaves from WT and *ecdr1* were fixed in 4% paraformaldehyde, dehydrated in an ethanol series and embedded in wax and subsequently exposed to TUNEL assay as described previously (Kim et al. 2011).

M. oryzae inoculation

A punch inoculation with slight modifications was performed as described previously (Wang et al. 2019). Briefly, blast isolates were cultured on oat meal agar medium for 7-10 d to generate spores. Spores were collected by washing the fungal agar cultures with ddH_2O (containing 0.2% Tween 20, Sigma), and the spore concentration of blast isolates was adjusted to 2×10^5 spores/mL. Detached top second leaves of two-week-old rice seedlings were wounded with a hole-punch. 7 μL of blast spore suspension was dropped to the injured area, and kept in a culture dish containing 0.1% 6-Benzylaminopurine. The inoculated leaves were kept in darkness at 28°C for 24 h, and then transferred to a controlled growth chamber (12 h light/12 h darkness at 28°C). Lesion size was measured at 7 days after incubation. Relative fungal growth (*MoPot*/*UBQ*) was measured using qRT-PCR

Xoo inoculation

Rice plants at heading stage were inoculated with *Xoo* isolates P2, P6, C5 and T1 by the leaf- clipping method (Wang et al. 2014). *Xoo* isolates were cultured on peptone sucrose agar plates supplemented with 20 mg/L cephalexin for two days, then washed off and re-suspended in sterilized water. The concentration of bacterial suspension was adjusted to an OD600 of 0.8 for inoculation. The distal tips (about 3 cm) of flag leaves were removed

using scissors pre-dipped with the bacterial suspension. 10 individual plants and three tillers per plant were inoculated. Lesion lengths were measured at 14 days after inoculation.

Map-based cloning

To map the *ECDR1* gene, a total of 559 F_2 typical *ecdr1*-type individuals were screened from a cross between *ecdr1* and *indica* cv. CO39 using molecular markers kept or newly developed in the lab. PCR amplification and gene sequencing analysis were employed to identify the candidate gene.

Vectors constructions and transformation

For the complementation experiments, the genomic fragments of *ORF4* and *ORF5* in WT including the entire coding region, 2500 bp upstream sequence and 800 bp downstream sequence were inserted into the pCAMBIA1305 vector. Subsequently, the recombined vectors were introduced into *Agrobacterium tumefaciens* strain EHA105 to infect *ecdr1* calli. The full-length coding region of *ECDR1* was amplified and cloned into pCUbi1390 vector to generate the overexpression vector of *ECDR1* driven by the ubiquitin promoter, and introduced into *ecdr1* calli by *Agrobacterium tumefaciens*-mediated transformation. To determine the functional domain of *ECDR1*, the cDNA fragments of 1-600 bp (spanning the amino acids 1-200), 601-1284 (spanning the amino acids 201-428), 1-900 bp (spanning the amino acids 1-300), 301-1284 bp (spanning the amino acids 101-428) and 174-1233 bp (spanning the entire hyccin domain) were amplified and cloned into the downstream of ubiquitin promoter in pCUbi1390 vector, respectively. All the resulting plasmids were subsequently introduced into *ecdr1* calli by *Agrobacterium tumefaciens*-mediated transformation. The entire coding regions of *ECDR1* homologs were amplified from *Zea mays*, *Setaria italica, Glycine max* and *Arabidopsis thaliana* and recombined into pCUbi1390 vectors. Subsequently, the recombined constructs were introduced into the *Agrobacterium tumefaciens* strain EHA105 and used to infect *ecdr1* calli.

Promoter activity assay

To determine promoter activities, the promoter region of *ECDR1* from WT and *ecdr1,* and the deleted 113 bp were cloned into the LUC vector (pGreenII 0800-LUC), which contained a *Renilla* reporter gene as an internal driven by the cauliflower mosaic virus (CaMV) *35S* promoter. The recombined plasmids were introduced into *Agrobacterium tumefaciens* strains EHA105, and then transiently expressed in *N. benthamiana* leaves as described previously (Meng et al. 2021). The LUC activity was represented by the ratio of LUC/Ren using the Promega Kit (E2920) following the manufacturer's instruction during 48-72 h after transformations.

Haplotype analysis

All SNPs in the promoter region (2 kb) of *ECDR1* and 3K rice accessions agronomic traits were acquired from the Rice SNP Seek Database (https://snp-seek.irri.org/_download.zul). Phenotypic differences among major *ECDR1* promoter haplotypes were analyzed by using one-way ANOVA followed by Duncan's multiple range test.

Phylogenetic analysis

Homolog proteins of ECDR1 were identified by searching the National Center for Biotechnology Information database (https://www.ncbi.nlm.nih.gov/) using ECDR1 protein sequence as query. Multiple sequences alignment was implemented using DNAMAN. The function domain of ECDR1 was predicted using Simple Modular Architecture Research Tools (SMART) (http://smart.embl-heidelberg.de/smart/set_mode.cgi?NORMAL=1). Phylogenetic tree was constructed using MEGA5.2 with the neighbor-joining statistical method and 1000 bootstrap replicates.

RNA extraction and real-time PCR analysis

RNA isolation and qRT-PCR assays were conducted as described previously (Meng et al. 2021). Total RNA was extracted from rice tissues using a Quick-RNA^{TM} Plant RNA MiniPrep Kit (Zymo Research) according to the manufacturer's instructions. For qRT-PCR, total RNA (2 μg) was reversely transcribed to cDNA using the Fast Quant RT Kit (Tiangen, Beijing, China). The qRT-PCR assay was performed using a SYBR Premix Ex TaqTM kit (TaKaRa) and an ABI prism

7500 Real-Time PCR System. The rice ubiquitin gene (*LOC_Os03g13170*) was used as an endogenous control, and the $2^{-\Delta\Delta CT}$ method was used to evaluate relative level of gene expression. The primers used for qRT-PCR was designed with GenScript (https://www.genscript.com/tools/real-time-pcr-taqman-primer-design-tool).

Subcellular localization of ECDR1

To detect the subcellular localization of ECDR1, the coding sequences of *ECDR1* without the stop codon was recombined into N-terminal of green fluorescent protein (GFP) in the pAN580 vector under the control of CaMV *35S* promoter. The fusion expression vectors were co-transformed into rice protoplasts with the plasma membrane marker Sacmp1-mCherry. A laser confocal scanning microscopy (ZEISS Microsystems LSM 700) was used to detect fluorescence signals.

Yeast two-hybrid assay

The standard Y2H assays were conducted using the MatchMaker GAL4 Two-Hybrid System (Clontech) following the manufacturer's instructions. The coding sequences of targeting genes were cloned into the pGADT7 or pGBKT7 vectors (Clontech), and various combinations of plasmids were co-transformed into the yeast AH109 strain. Positive transformants were selected on synthetic drop-out (SD) medium lacking Trp and Leu (DDO), while the screening of interactions was performed on SD medium lacking Trp, Leu, His, and Ade (QDO). The experiments were performed at least three times independently.

The split-ubiquitin Y2H assays were performed using the DUAL hunter system (Dual systems Biotech). The process of Y2H assay was conducted according to the method described previously (You et al. 2016). The full coding sequences of the corresponding genes were fused to the Nub fragment in the pXGY17 vector or to the Cub fragment in the pXGY18 vector, respectively. Test constructs were transformed into the yeast strain NMY51 according to the manufacturer's instructions. The growth state of each transformant was examined on the QDO (SD/-Trp/-Leu/-His/-Ade) medium.

Firefly LCI assay

The luciferase complementation assay was performed in *N.benthamiana* leaves as previously described (Zhou et al., 2018). Briefly, the coding sequences of *ECDR1*, *PI3K1*, and *PI4K1* were fused to the upstream of N terminus of LUC (nLUC) in the pCAMBIA-nLUC vector, while the coding sequences of *TPR1* and *TPR2* were fused to the downstream of C terminus of LUC (cLUC) in the pCAMBIA-cLUC vector. These constructs were transformed into the EHA105 strain, and various combinations of EHA105 strains were infiltrated into *N.benthamiana* leaves. The LUC image was captured using low-light-cooled CCD imaging apparatus (NightSHADE LB 985 [Berthold] with Indigo software) during 48-72 h after infiltration. The nLUC-PAA2 and cLUC-PAA2 vectors were used as negative controls in LCI assays.

BiFC assay

For the BiFC assays, the coding sequences of *TPR1*, *TPR2* and *ECDR1* were cloned into N-terminal YFP (YN) to generate YN-TPR1, YN-TPR2 and YN-ECDR1, and the full-length of *ATG6A* and *ATG6B* were cloned into C-terminal YFP to generate YC-ATG6A, YC-ATG6B. These constructed vectors were then transformed into the EHA105 strain, and various combinations of EHA105 strains were used to infiltrate *N. benthamiana* leaves. After 2 to 3 d, the fluorescence signals were captured using an LSM880 laser scanning confocal microscope.

Co-IP assay in *N. benthamiana*

The Co-IP assay was conducted according to the method described previously (You et al. 2019). The coding sequences of *TPR1*, *TPR2* and *VPS34*, *ECDR1*, *PI4Kα1* were separately cloned into the pCAMBIA1305-GFP and pCAMBIA1300-221-Flag vectors to generate TPR1/2-GFP, ECDR1-Flag, VPS34-Flag, and PI4Kα1-Flag fusions. The plasmids were transiently expressed in *N. benthamiana* leaves via Agrobacterium-mediated transfection. After 2 to 3 days, total protein was extracted from freshly harvested leaves in triple volumes of NB1 buffer (50 mM Tris-MES, pH = 8.0, 1 mM $MgCl_2$, 0.5 M sucrose, 10 mM EDTA, 5 mM DTT) added to proteinase inhibitor cock-tail (Roche, 04693132001). The supernatant was collected after centrifugation 12000 rpm 30 min at 4℃ and precleared with protein G-Agarose (Roche, 11243233001) for 1 h. The plant extracts were incubated with GFP magnetic beads (MBL, D153-11) at 4℃ at least for 4 h. The magnetic beads were

rinsed three times with the NB1 buffer and then boiled in the 2 × SDS-PAGE sample buffer for immunoblot analysis. Anti-GFP (MBL, 598-7) or anti-Flag (MBL, M185-7) antibodies at 1:2000 dilutions were used for the detection.

PI3k and PI4K activity inhibition assay

25-day-old seedlings were used for PI3K and PI4K activity inhibition assays. Wortmannin (HY-10197), LY294002 (HY-10108) and PAO (HY-106012) were purchased from MedChemExpress. All stock solutions (100 mM) were made in 100% DMSO, and were diluted in water into different concentration for each treatment assay. To assess the roles of PI3K and PI4Kα1 activities in cell death, seedlings were treated by a spray application of the following inhibitors which were dissolved in a solution containing 0.02% (v/v) Silwet L-77: Wortmannin (200 μM), LY294002 (200 μM), phenylarsine oxide (PAO, 200 μM), or a combination of LY294002 and PAO (200 μM each). Seedlings sprayed with a DMSO solution were used as the control. For the experiment to investigate the Wort effect on rice blast resistance, the second leaves of two-week-old rice seedlings were detached and soaked in a 0.1% 6-Benzylaminopurine (6-BA) solution containing 100 μM Wort, followed by pathogen inoculation as described previously (Wang et al. 2019).

Measurement of PI3P and PI4P content in leaf

The cellular levels of PI3P and PI4P were quantified using commercial ELISA-based detection kits (Xu et al. 2026; Guo et al. 2020). Briefly, approximately 0.1 g of leaves from 30-day-old seedlings was ground in liquid nitrogen, followed by addition of 250 μL extraction buffer containing 50 mM Tris-HCl (pH 7.4), 150 mM NaCl, 1 mM EDTA, 1% Triton X-100, and 1× protease inhibitor cocktail (B14001, Selleck). The mixture was extracted on a shaker at 4°C for 30 min and then centrifuged at 12,000 g for 20 min at 4°C. The supernatant was collected for subsequent analysis. The contents of PI3P and PI4P were measured using the PI3P detection kit (LM8K957O, SHANG HAI LMAI Bio), the PI4P detection kit (LM8K978O, SHANG HAI LMAI Bio), respectively.

Primers

All the primers used in this study were listed in Supplemental Table S9.

Statistical analysis

Statistical analysis was conducted using GraphPad Prism 8. Data are presented as mean ± SD, and *n* indicates numbers of samples and biological replicates. A two-sided unpaired Student's *t*-test was used to assess significant differences between two groups. For comparisons involving three or more groups, one-way analysis of variance (ANOVA) followed by Duncan's multiple range test was applied.

Accession numbers

Sequence data for this article can be found in GenBank/EMBL data libraries under the following accession number: *ECDR1* (*LOC_Os11g06860*), *PI3K1* (*LOC_Os05g08810*), *PI3K2* (*LOC_Os08g21590*), *PI4K1* (*LOC_Os03g50320*), *TPR1* (*LOC_Os10g33290*), *TPR2* (*LOC_Os12g37780*), *ATG6A* (*LOC_Os01g48920*), *ATG6B* (*LOC_Os03g15290*).

Funding information

This work was supported by the Central Public-interest Scientific Institution Basal Research Fund (Y2026YC02), the National Natural Science Foundation of China (32072411), the National Key Research and Development Program of China (2022YFD1201504), the Fundamental Research Funds of CAAS (Y20n24YJ12), the Biological Breeding-National Science and Technology Major Project (2023ZD04070), the Basic Research Center, Innovation Program of Chinese Academy of Agricultural Sciences (CAAS-BRC-CS-2025-02), and the Inner Mongolia Innovation Center of Biological Breeding Technology.

Acknowledgments

We thank Dr. Chunlian Wang and Dr. Zhiyuan Ji, Institute of Crop Sciences, CAAS, for kindly providing the *Xoo* strains and technical guidance.

Author Contribution

Jianmin Wan, Cailin Lei and Shanshan Zhu conceived and designed the experiments. Zhichao Zhao provided the *ecdr1* mutant materials. Shuang Zhang, Lingzhi Meng,

Changyan Qi, Chen Xie. And Xiaokang Jiang performed the experiments. Yulong Ren, Jie Wang, Zhijun Cheng, Xin Wang, and Xiuping Guo provided technical assistance and completed the field work. Shuang Zhang and Lingzhi Meng and Cailin Lei drafted the manuscript. Jianmin Wan, Cailin Lei, Shanshan Zhu and Ling Jiang revised the manuscript.

Conflict of interest

The authors declare that they have no conflicts of interest.

Data availability

The data used to support the findings of this study are available upon request to the corresponding author.

Figure Legends

Figure 1. Phenotypic characterization of wild-type (WT) and *ecdr1*. A) Trypan blue staining assay to detect cell death. **B)** Terminal deoxynucleotidyl transferase dUTP nick end labeling (TUNEL) assay to detect nuclear DNA degradation. Red fluorescence represents propidium iodide (PI) staining and green fluorescence indicates TUNEL-positive signal, an indicator for DNA fragmentation. Bars, 50 μm. **C)** 3,3'-Diaminobenzidine (DAB) staining assay to detect H_2O_2. **D)** Nitro blue tetrazolium (NBT) staining assay to detect $O_2^{\cdot -}$ accumulation. **E)** The measurement of reactive oxygen species (ROS) contents in WT and *ecdr1*. **F)** Quantitative real-time PCR (qRT-PCR) analysis of defense-related genes in WT and *ecdr1* mutant at 14 days after sowing (DAS) and 28 DAS. **G)** The *ecdr1* mutant showed enhanced resistance to blast isolates 99-26-2 and Zhong 10-8-14. Bar, 1 cm. **H)** Lesions lengths of WT and *ecdr1* after punch inoculation with the *M. oryzae* strain 99-26-2 and Zhong 10-8-14 **I)** Relative fungal growths of WT and *ecdr1* after punch inoculation with the *M. oryzae* strain 99-26-2 and Zhong 10-8-14. **J)** The *ecdr1* mutant enhanced resistance to *Xanthomonas oryzae* pv. *oryzae* (*Xoo*) isolates P2, P6, C5 and T1 compared to WT. Bar, 2 cm. **K)** Bacterial blight lesion lengths of WT and *ecdr1* plants against P2, P6, C5 and T1. In boxplot (H, K), boxes represent the interquartile range, center lines indicate medians, and whiskers extend to the minima and maxima. Significance differences were determined by

Student's *t* test (*n* =15; ***P* < 0.01). In (E, F, I), data are presented as mean ± SD and the statistically significant differences are determined by Student's *t* test (*n* = 3; ***P* < 0.01).

ALT TEXT: Graphs depicting phenotypes of wild-type and *ecdr1*, with subfigures labelled from A to K, illustrating *ecdr1* is an autoimmunity mutant with enhanced resistance to both fungal and bacterial diseases.

Figure 2. Map-based cloning of *ECDR1*. A) Fine mapping of *ECDR1*. Molecular markers and numbers of recombinants are labeled above and below the filled bars, respectively. Candidate *ORF4* and *ORF5* are marked in red. Chr.11, chromosome 11. Rec, recombinant. **B)** Sequence comparisons of *ORF4* and *ORF5* between WT and *ecdr1*. ATG denotes *ORF4* start codon; TGA denotes *ORF5* stop codon. The blue line represents 546 bp deletion in *ecdr1* compared to WT. The red line represents *mping* transposon. The blue and red boxes represent the 99 bp and 14 bp sequences separated by *mping*. **C)** Transgenic complementation of *ORF4*. 4#1 and 4#2, two independent transgenic positive individuals of *ORF4*. Bar, 15 cm. **D)** Resistance of WT, *ecdr1* mutant and *ECDR1*-complementaion plants to *Xanthomonas oryza*e pv. *oryzae* (*Xoo*) strains C5 and P2. Bars, 2 cm. **E)** Lesion lengths of WT, *ecdr1* mutant and *ECDR1*-complementaion plants (*n* =15). **F)** The 433 bp insertion (*mping*) in WT from KD2016 evidenced by agarose gel electrophoresis. KD2016, Kendao 2016; CY, Chunyang; ZH11, Zhonghua11; NIP, Nipponbare. **G)** Luciferase transient assay. Left constructs, schematic representation of the reporter constructs. Four constructs with WT promoter (P^{WT}), WT promoter with a 433 bp *(ming*) deletion ($P^{WT\,\Delta\,433\,bp}$), *ecdr1*-type promoter (P^{ecdr1}), the 113 bp sequence (P*113*) were introduced into *Nicotiana benthamiana* leaves. Data are presented as mean ± SD and the significant differences are determined by Student's *t* test (*n* = 3, ***P* < 0.01). **H)** Expression analysis of *ECDR1* in WT, *ecdr1* mutant and NIP (*n*=3). In boxplot (E), boxes represent the interquartile range, center lines indicate medians, and whiskers extend to the minima and maxima. In (G, H), data are presented as mean ± SD. One-way ANOVA with Duncan's multiple range test was applied for statistical analysis (*P* < 0.01; different letters indicate significant differences among groups).

ALT TEXT: Graphs depicting the cloning and biological function of *ECDR1*, with subfigures labelled from A to H., demonstrating that *ORF4* was the functional *ECDR1* gene, in which the 113 bp deletion is responsible for the autoimmunity phenotype and enhanced disease resistance in *ecdr1*.

Figure 3. Expression and phylogenetic analysis of ECDR1 in different species. A) Relative expression of *ECDR1* in various tissues including root of 7-day-old seedling, stem, flag leaf, panicle and leaf sheath of WT and *ecdr1* plants at heading stage. **B)** *ECDR1* expression levels in different leaf blades. 1L-5L represent the leaves from base to top of main tiller at five-leaf stage. **C)** Subcellular localization of ECDR1 protein. ECDR1-GFP, ECDR1 fused to GFP; SCAMP1-mCherry, plasma membrane marker. Bars, 5 μm. **D)** Phylogenetic analysis of ECDR1 in plants. The species in yellow background and green background represent dicots and monocots, respectively. The tree was constructed using MEGA 5.2 and bootstrapped with 1000 replicates. In (A, B), data are presented as mean ± SD and the significance differences were determined by Student's *t* test ($n = 3$; $^{**}P < 0.01$).

ALT TEXT: Graphs and microscopic images depicting expression and phylogeny of ECDR1 in different species, with subfigures labelled from A to D, demonstrating ECDR1 was a plasma membrane-located protein and closest to *Brachypodium distachyon* BRADI_4g24260v3.

Figure 4. *ECDR1* encodes a highly conservative hyccin-containing protein. A) Amino acid sequences comparison of ECDR1 in monocots including *Oryza Sativa*, *Brachypodium distachyon*, *Zea mays*, *Setaria italica*, *Sorghum bicolor* and dicots containing *Glycine max*, *Arabidopsis thaliana*. The consensus amino acid residues are shown at the bottom with lowercases letters. Black indicates 100% identity; red indicates >75% identity; green indicates >50% identity; yellow indicates >33% identity. **B)** Schematic representation of the various truncated visions of ECDR1 proteins. $ECDR1^{1\text{-}200}$, $ECDR1^{201\text{-}428}$, $ECDR1^{1\text{-}300}$, $ECDR1^{101\text{-}428}$ and $ECDR1^{Hyccin}$ encode amino acids 1-200, 201-428, 1-300, 101-428 and the hyccin domain of ECDR1, respectively. The hyccin domain is indicated with green box. **C)** The overexpression plants of $ECDR1^{hyccin}$ in *ecdr1* recovered WT phenotype. Bar, 15 cm. **D)** Overexpression of *ECDR1* homologs from different species in *ecdr1*. ZM, SI, GM and AT

denote overexpression of *ECDR1* homologs from *Zea mays*, *Setaria italica*, *Glycine max* and *Arabidopsis thaliana*, respectively. Bar, 15 cm.

ALT TEXT: Graphs depicting the function of the hyccin domain in ECDR1, with subfigures labelled from A to D, showing high conservativeness of ECDR1 in function among plants.

Figure 5. The interactions of TPR1 and TPR2 (TPR1/2) with ECDR1, PI3K1, and PI4K1. A) Split-ubiquitin membrane yeast two-hybrid assay revealed that while TPR1 and TPR2 specifically interacted with ECDR1, PI3K1, and PI4K1, no detectable interactions were observed for TPR3, TPR4, or TPR5 with these proteins. DDO, SD/-Trp/-Leu; QDO, SD/-Trp/-Leu/-His/-Ade. Cub, the C-terminal half of ubiquitin; Nub, the N-terminal half of ubiquitin. **B)** The LCI assay confirmed the interactions of TPR1/2 with ECDR1, PI3K1, and PI4K. CL, C terminus of LUC; NL, N terminus of LUC. CL-PPA2 and NL-PPA2 were used as negative controls. **C** to **E)** Co-IP assay showed that ECDR1-Flag **C)**, PI3K1-Flag **D)**, and PI4K1-Flag **E)** can be coimmunoprecipitated in the total leaf extract of *Nicotiana benthamiana* with TPR1/2-GFP. **F)** ECDR1 interacted with TPR1 or TPR2 via the hyccin domain.

ALT TEXT: Graphs depicting the interactions of TPR1/2 with ECDR1, PI3K1 and PI4K1, with subfigures labelled from A to F, showing that ECDR1 acted as a new component in rice PI4K1 and PI3K1 complexes.

Figure 6. ATG6 interacted with ECDR1, TPR1 and TPR2. A) Standard Y2H assays showed that ATG6 interacted with ECDR1 and TPR1/TPR2. **B)** Bimolecular Fluorescence Complementation (BiFC) assays for the determining interaction of ATG6 with ECDR1, TPR1/TPR2. Bar, 5 μm. **C to F)** CRISPR/Cas9-mediated editing of *ECDR1*, *PI3K1*, *TPR1* and *TPR2*. Plus (+) and minus (-) signs indicated base insertion (in blue) and deletion (by hyphen), respectively, relative to wild-type (WT). Gray boxes denote coding sequences, and gray lines are the untranslated regions and introns. The positions of the protospacer adjacent motif sequences are indicated in red. The primers used for gene knockout are underlined.

ALT TEXT: Graphs depicting the interaction of ATG6 with ECDR1, TPR1 and TPR2, and the gene-editing sites of *ECDR1*, *TPR1/2* and *PI3K1* in rice, with subfigures labelled from A to F, demonstrating the direct interaction of both ECDR1 and TPR1/2 with ATG6A/B.

Figure 7. The PI3K and PI4K inhibitors could trigger cell death, and immunity. Wort aggravated lesion symptoms on day 2 **A)** and day 4 **B)** after treatments in *ecdr1* mutant. Dimethyl Sulfoxide (DMSO) and Wortmannin (Wort) represent the *ecdr1* mutant leaf blades treated with DMSO (control) and wortmannin (200 μM), respectively. Bars, 3 cm. **C)** Trypan blue staining for cell death on the 2nd and 4th days after treatments with wortmannin in *ecdr1*. Bars, 1 cm. **D)** PAO and LY294002 aggravated lesion symptoms on day 7 after treatments. PAO and LY represent the *ecdr1* mutant leaf blades treated with PI4K-specific inhibitor PAO (200 μM) and PI3K-specific inhibitor LY294002 (200 μM), respectively. Bars, 3 cm. **E)** PI3P and **F)** PI4P content in leaf tissue of WT and *ecdr1* mutant. **G)** Wort promoted the lesion initiation and development in 10-day-old WT seedlings. Bar, 1 cm. **H)** WT plants pre-treated with Wort showed enhanced resistance to blast. Bar, 1cm. **I to J)** Lesions lengths and relative fungal growths of wort-treated WT and control after punch inoculation with the *M. oryzae* strains. In (E, F, J), data are presented as mean ± SD. Significant differences are determined by Student's *t* test ($n = 3$; $^{**}P < 0.01$). In boxplot (I), boxes represent the interquartile range, center lines indicate medians, and whiskers extend to the minima and maxima. Significant differences were determined by Student's *t* test ($n = 15$; $^{**}P < 0.01$).

ALT TEXT: Graphs depicting the association of the cell death and immunity in *ecdr1* with the activity inhibition of PI3K1 and PI4K1, with subfigures labelled from A to J, demonstrating that simultaneous inhibition of PI3K1 and PI4K1 activities was responsible for the autoimmunity phenotype in *ecdr1*.

Figure 8. A working model that ECDR1 regulates cell death and disease resistance in rice. In wild-type (WT), functional ECDR1 can interact with PI3K1 and PI4K1 to form the PI3K1 and PI4K1 complex, respectively, leading to the production of PI3P and PI4P, which thereby maintains normal growth and development. However, a 113 bp deletion in the promoter of ECDR1 results in reduced expression of this gene, leading to decreased enzymatic activity of PI3K and PI4K, as well as decreased biosynthesis of PI3P and PI4P, which ultimately triggers a plant autoimmunity phenotype and enhances plant disease resistance. Simultaneous inhibition of PI3K1 and PI4K1 activities in WT can result in

reduced PI3P and PI4P levels, leading to similar autoimmunity phenotype and defense response as *ecdr1*. The PI3K1 complex comprises ECDR1, ATG6, TPR1/2, PI3K1 and VPS15. The PI4K1 complex comprises ECDR1, TPR1/2, and PI4K1. Direct physical interactions of proteins are indicated by solid lines, and indirect interactions by dashed lines.

ALT TEXT: Graphs depicting the working model that ECDR1 regulates cell death and disease resistance in rice, showing that the ECDR1 mutation suppressed PI3K1 and PI4K1 activities and caused decreased PI3P and PI4P levels, ultimately leading to the cell death and enhanced disease resistance in *ecdr1*.

Reference

Akhter, S., Uddin, M.N., Jeong, I.S., Kim, D.W., Liu, X.M., and Bahk, J.D. (2016) Role of Arabidopsis AtPI4Kγ3, a type II phosphoinositide 4-kinase, in abiotic stress responses and floral transition. Plant Biotechnol J, **14**, 215–230.

Baskin, J.M., Wu, X., Christiano, R., Oh, M.S., Schauder, C.M., Gazzerro, E., et al. (2016) The leukodystrophy protein FAM126A (hyccin) regulates PtdIns (4) P synthesis at the plasma membrane. Nat Cell Biol, **18**, 132–138.

Batrouni, A.G., Bag, N., Phan, H.T., Baird, B.A., and Baskin, J.M. (2022) A palmitoylation code controls PI4KIIIα complex formation and PI (4,5) P2 homeostasis at the plasma membrane. J Cell Sci, **135**, jcs259365.

Bhati, K.K., Luong, A.M., and Batoko, H. (2021) VPS34 complexes in plants: Untangled Enough? Trends Plant Sci, **26**, 303–305.

Bruggeman, Q., Raynaud, C., Benhamed, M., and Delarue, M. (2015) To die or not to die? Lessons from lesion mimic mutants. Front Plant Sci, **6**, 24.

Chakraborty, J., Ghosh, P., and Das, S. (2018) Autoimmunity in plants. Planta, **248**, 751–767.

Chen, H., Liu, L., Zhou, Q., Zhu, Y., Gao, Z., Zhu, T., et al. (2025) Lesion mimic mutant: an ideal genetic material for deciphering the balance between plant immunity and growth. Rice (N Y), **18**, 34.

Dornan, G.L., Dalwadi, U., Hamelin, D.J., Hoffmann, R.M., Yip, C.K., and Burke, J.E. (2018) Probing the Architecture, Dynamics, and Inhibition of the PI4KIIIα/TTC7/FAM126 Complex. J Mol Biol, **430**, 3129–3142.

Etkovitz, N., Rubinstein, S., Daniel, L., and Breitbart, H. (2007) Role of PI3-kinase and PI4-kinase in actin polymerization during bovine sperm capacitation. Biol Reprod, **77**, 263–273.

Fang, R., Jiang, Q., Jia, X., Jiang Z. (2023) ARMH3-mediated recruitment of PI4KB directs Golgi-to-

endosome trafficking and activation of the antiviral effector STING. Immunity, **56**, 500–515.

Fitzgerald, H.A., Chern, M.S., Navarre, R., and Ronald, P.C. (2004) Overexpression of (At)NPR1 in rice leads to a BTH- and environment-induced lesion-mimic/cell death phenotype. Mol Plant Microbe Interact, **17**, 140–151.

Fujimoto, M., Suda, Y., Vernhettes, S., Nakano, A., and Ueda, T. (2015) Phosphatidylinositol 3-kinase and 4-kinase have distinct roles in intracellular trafficking of cellulose synthase complexes in *Arabidopsis thaliana*. Plant Cell Physiol, **56**, 287–298.

Fujiwara, T., Maisonneuve, S., Isshiki, M., Mizutani, M., Chen, L., Wong, H.L., et al. (2010) Sekiguchi lesion gene encodes a cytochrome P450 monooxygenase that catalyzes conversion of tryptamine to serotonin in rice. J Biol Chem, **285**, 11308–11313.

Funderburk, S.F., Wang, Q.J., and Yue, Z. (2010) The Beclin 1-VPS34 complex-at the crossroads of autophagy and beyond. Trends Cell Biol, **20**, 355–362.

Gao, M., He, Y., Yin, X., Zhong, X., Yan, B., Wu, Y., et al. (2021) Ca^{2+} sensor-mediated ROS scavenging suppresses rice immunity and is exploited by a fungal effector. Cell, **184**, 5391–5404.e17.

Gui, X., Yang, H., Li, T., Tan, X., Shi, P., Li, M., et al. (2019) Autophagy induction via STING trafficking is a primordial function of the cGAS pathway. Nature, **567**, 262–266.

Harrison-Lowe, N.J. and Olsen, L.J. (2008) Autophagy protein 6 (ATG6) is required for pollen germination in *Arabidopsis thaliana*. Autophagy, **4**, 339–348.

Heath, M.C. (2000) Hypersensitive response-related death. Plant Mol Biol, **44**, 321–334.

Hsu, Y. W., Juan, C. T., Guo, C. L., Wang, H. J., and Jauh, G. Y. (2025) HYCCIN2 is essential for recruiting the SH3P2-DRP1A complex to the cell plate in Arabidopsis embryos. New Phytol, **247**, 2781–2796.

Ischebeck, T., Seiler, S., and Heilmann, I. (2010) At the poles across kingdoms: phosphoinositides and polar tip growth. Protoplasma, **240**, 13–31.

Jiang, N. and Wessler, S.R. (2001) Insertion preference of maize and rice miniature inverted repeat transposable elements as revealed by the analysis of nested elements. Plant Cell, **13**, 2553–2564.

Kim, S.G., Kim, S.T., Wang, Y., Yu, S., Choi, I.S., Kim, Y.C., et al. (2011) The RNase activity of rice probenazole-induced protein1 (PBZ1) plays a key role in cell death in plants. Mol Cells, **31**, 25–31.

Lam, E., Kato, N., and Lawton, M. (2001) Programmed cell death, mitochondria and the plant hypersensitive response. Nature, **411**, 848–853.

Lee, H.N., Zarza, X., Kim, J.H., Yoon, M.J., Kim, S.H., Lee, J.H., et al. (2018) Vacuolar Trafficking Protein VPS38 Is Dispensable for Autophagy. Plant Physiol, **176**, 1559–1572.

Lee, Y., Bak, G., Choi, Y., Chuang, W.I., Cho, H.T., and Lee, Y. (2008) Roles of phosphatidylinositol 3-kinase in root hair growth. Plant Physiol, **147**, 624–635.

Lee, Y., Kim, E.S., Choi, Y., Hwang, I., Staiger, C.J., Chung, Y.Y., and Lee, Y. (2008) The Arabidopsis phosphatidylinositol 3-kinase is important for pollen development. Plant Physiol, **147**, 1886–1897.

Lees, J.A., Zhang, Y., Oh, M.S., Schauder, C.M., Yu, X., Baskin, J.M., et al. (2017) Architecture of the

human PI4KIIIα lipid kinase complex. Proc Natl Acad Sci U S A, **114**, 13720–13725.

Leprince, A.S., Magalhaes, N., De Vos, D., Bordenave, M., Crilat, E., Clément, G., et al. (2014) Involvement of Phosphatidylinositol 3-kinase in the regulation of proline catabolism in *Arabidopsis thaliana*. Front Plant Sci, **5**, 772.

Liu, F., Hu, W., Li, F., Marshall, R.S., Zarza, X., Munnik, T., and Vierstra, R.D. (2020) AUTOPHAGY-RELATED14 and its associated Phosphatidylinositol 3-Kinase complex promote autophagy in Arabidopsis. Plant Cell, **32**, 3939–3960.

Liu, F., Hu, W., and Vierstra, R.D. (2018) The Vacuolar Protein Sorting-38 subunit of the Arabidopsis Phosphatidylinositol-3-Kinase complex plays critical roles in autophagy, endosome sorting, and gravitropism. Front Plant Sci, **9**, 781.

Liu, B., Luo, S., Tian, W., Liu, X., Zhang, J., Ren, Y., et al. (2026). Perturbation of anion/cation transport leads to apical panicle abortion in rice by disrupting Ca^{2+} homeostasis. Plant Biotechnol J, **24**, 1503–1517.

Meng, L., Qi, C., Wang, C., Wang, S., Zhou, C., Ren, Y., et al. (2021) Determinant factors and regulatory systems for anthocyanin biosynthesis in rice apiculi and stigmas. Rice (N Y), **14**, 37.

Naito, K., Cho, E., Yang, G., Campbell, M.A., Yano, K., Okumoto, Y., et al. (2006) Dramatic amplification of a rice transposable element during recent domestication. Proc Natl Acad Sci U S A, **103**, 17620–17625.

Noack, L.C., Bayle, V., Armengot, L., Rozier, F., Mamode-Cassim, A., Stevens, F.D., et al. (2022) A nanodomain-anchored scaffolding complex is required for the function and localization of phosphatidylinositol 4-kinase alpha in plants. Plant Cell, **34**, 302–332.

Ohashi, Y., Tremel, S., and Williams, R.L. (2019) VPS34 complexes from a structural perspective. J Lipid Res, **60**, 229–241.

Okazaki, K., Miyagishima, S., and Wada, H. (2015) Phosphatidylinositol 4-phosphate negatively regulates chloroplast division in Arabidopsis. Plant Cell, **27**, 663–674.

Pemberton, J.G., Kim, Y.J., and Balla, T. (2020) Integrated regulation of the phosphatidylinositol cycle and phosphoinositide-driven lipid transport at ER-PM contact sites. Traffic, **21**, 200–219.

Pitsili, E., Phukan, U.J., and Coll, N.S. (2020) Cell death in plant immunity. Perspect Biol, **12**, a036483.

Qiao, Y., Jiang, W., Lee, J., Park, B., Choi, M.S., Piao, R., et al. (2010) *SPL28* encodes a clathrin-associated adaptor protein complex 1, medium subunit micro 1 (AP1M1) and is responsible for spotted leaf and early senescence in rice (*Oryza sativa*). New Phytol, **185**, 258–274.

Sašek, V., Janda, M., Delage, E., Puyaubert, J., Guivarc'h, A., López Maseda, E., et al. (2014) Constitutive salicylic acid accumulation in pi4kIIIβ1β2 Arabidopsis plants stunts rosette but not root growth. New Phytol, **203**, 805–816.

Shine, M.B., Xiao, X., Kachroo, P., and Kachroo, A. (2019) Signaling mechanisms underlying systemic acquired resistance to microbial pathogens. Plant Sci, **279**, 81–86.

Starodubtseva, A., Kalachova, T., Retzer, K., Jelínková, A., Dobrev, P., Lacek, J., et al. (2022) An Arabidopsis mutant deficient in phosphatidylinositol-4-phosphate kinases ß1 and ß2 displays altered auxin-related responses in roots. Sci Rep, **12**, 6947.

Steinfeld, N., Lahiri,V., Morrison,A., Metur, S.P., Klionsky, D.J., Weismana, L.S. (2021) Elevating PI3P drives select downstream membrane trafficking pathways. Mol Biol Cell, **32**, 143–156.

Stevenson-Paulik, J., Love, J., and Boss, W.F. (2003) Differential regulation of two Arabidopsis type III phosphatidylinositol 4-kinase isoforms. A regulatory role for the pleckstrin homology domain. Plant Physiol, **132**, 1053–1064.

Sha, G., Sun, P., Kong, X., Han, X., Sun, Q., Fouillen, L., et al. (2023). Genome editing of a rice CDP-DAG synthase confers multi pathogen resistance. Nature, **618**, 1017–1023.

Van Durme, M. and Nowack, M.K. (2016) Mechanisms of developmentally controlled cell death in plants. Curr Opin Plant Biol, **29**, 29–37.

Vanhaesebroeck, B., Leevers, S.J., Panayotou, G., and Waterfield, M.D. (1997) Phosphoinositide 3-kinases: a conserved family of signal transducers. Trends Biochem Sci, **22**, 267–272.

Wang C, Fan Y, Zheng C, Qin T, Zhang X, Zhao K. 2014. High resolution genetic mapping of rice bacterial blight resistance gene *Xa23*. Molecular Genetics and Genomics **289**, 745–753.

Wang, Jiachang, Liu, X., Zhang, A., Ren, Y., Wu, F., Wang, G., et al. (2019) A cyclic nucleotide-gated channel mediates cytoplasmic calcium elevation and disease resistance in rice. Cell Res, **29**, 820–831.

Wang, S., Lei, C., Wang, J., Ma, J., Tang, S., Wang, C., et al. (2017) *SPL33*, encoding an eEF1A-like protein, negatively regulates cell death and defense responses in rice. J Exp Bot, **68**, 899–913.

Xu, N., Gao, X.Q., Zhao, X.Y., Zhu, D.Z., Zhou, L.Z., and Zhang, X.S. (2011) Arabidopsis AtVPS15 is essential for pollen development and germination through modulating phosphatidylinositol 3-phosphate formation. Plant Mol Biol, **77**, 251–260.

Xu, S., Ma, M., Zhao, H., Zhou, A., Li, Z., Li, B., et al. (2026) OsVPS34-generated PI3P recruits GPA5/Rab5a to regulate post-Golgi glutelin trafficking in rice endosperm. Plant Physiology, kiag154. Advance online publication.

You, Q., Zhai, K., Yang, D., Yang, W., Wu, J., Liu, J.Z., et al. (2016) An E3 ubiquitin ligase-BAG protein module controls plant innate immunity and broad-spectrum disease resistance. Cell Host Microbe, **20**, 758–769.

You, X., Zhu, S., Zhang, W., Zhang, J., Wang, C., Jing, R., et al. (2019) OsPEX5 regulates rice spikelet development through modulating jasmonic acid biosynthesis. New Phytol, **224**, 712–724.

Zhang, X. and Dong, X. (2022) Life-or-death decisions in plant immunity. Curr Opin Immunol, **75**, 102–169.

Zhang, B.C., Nandakumar, R., Reinert, L.S., Huang, J., Laustsen, A., Gao, Z.L., et al. (2020) STEEP mediates STING ER exit and activation of signaling. Nat. Immunol., **21**, 868–879.

Zhao, C.Y. and Xue, H.W. (2020) PI4Kγ2 Interacts with E3 Ligase MIEL1 to regulate auxin metabolism and root development. Plant Physiol, **184**, 933–944.

Zheng, Y., Zhang, X., Gao, C. (2023) PI4P STimulatING innate immune activation: beyond the Golgi. Cell Mol Immunol., **20**, 1399–1400.

Zhou, Z., Bi, G., and Zhou, J.M. (2018). Luciferase complementation assay for protein-protein interactions in plants. Curr Protoc Plant Biol., **3**, 42–50.

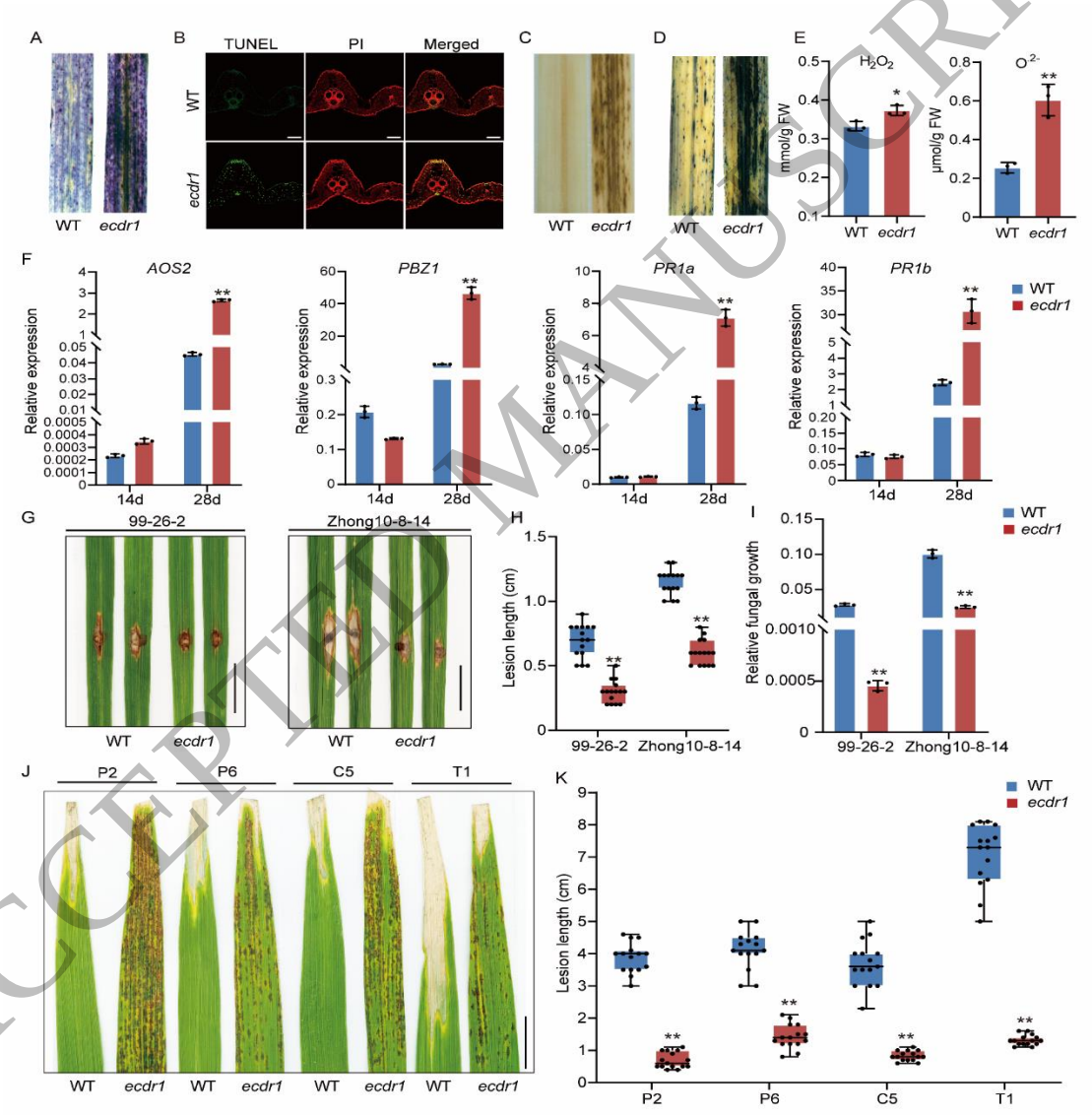

Figure 1
210x244 mm (x DPI)

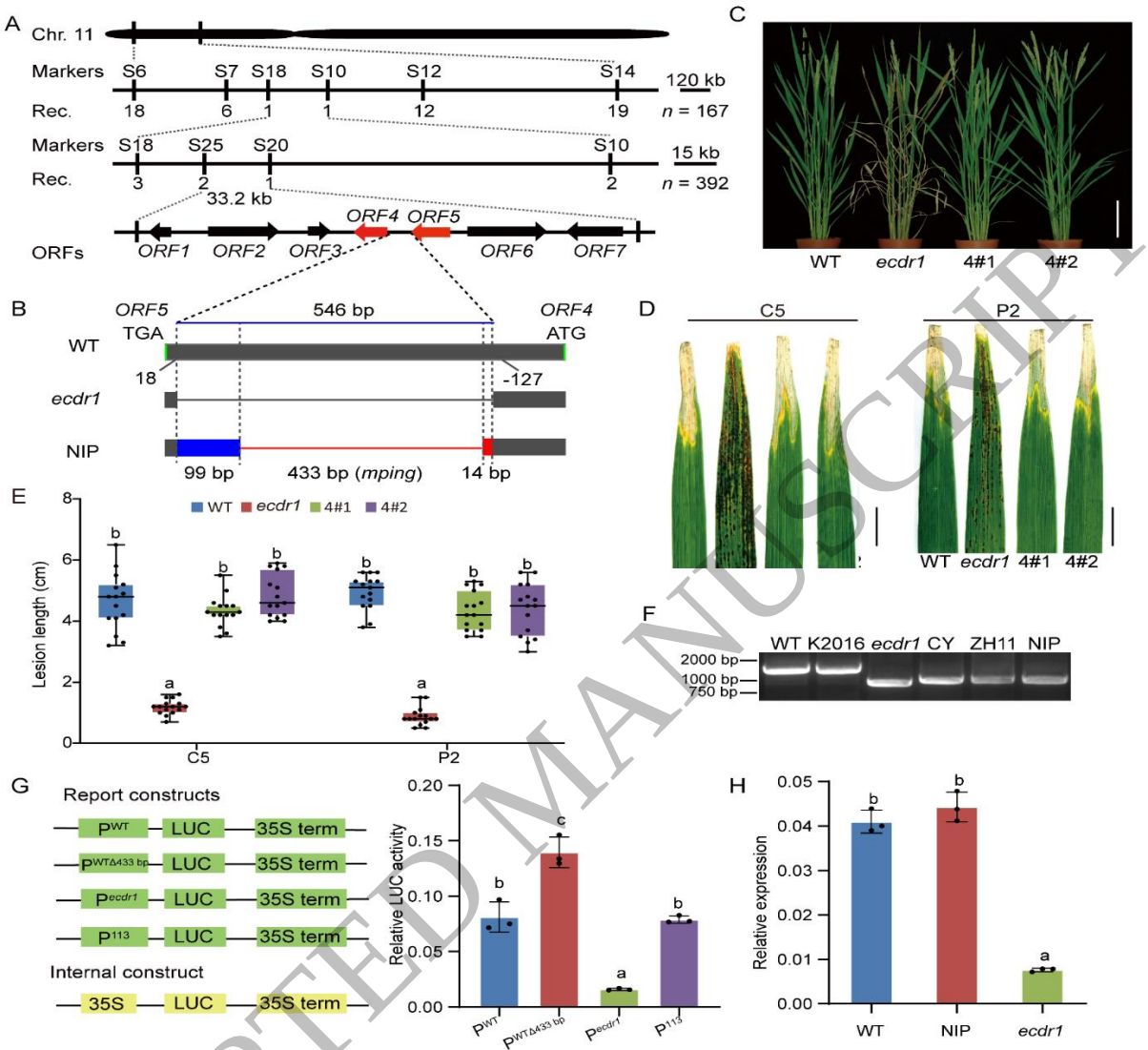

Figure 2
210x222 mm (x DPI)

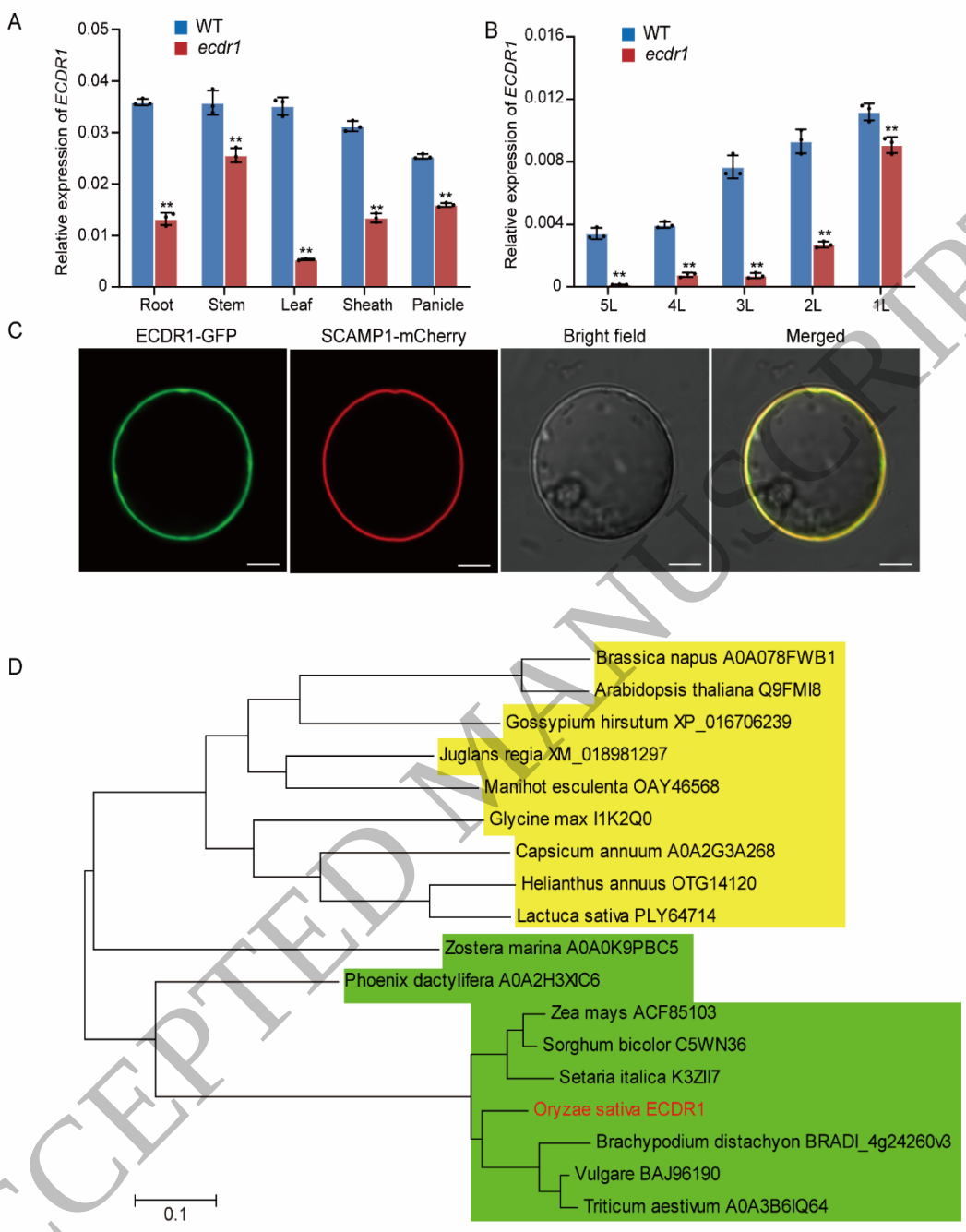

Figure 3
210x232 mm (x DPI)

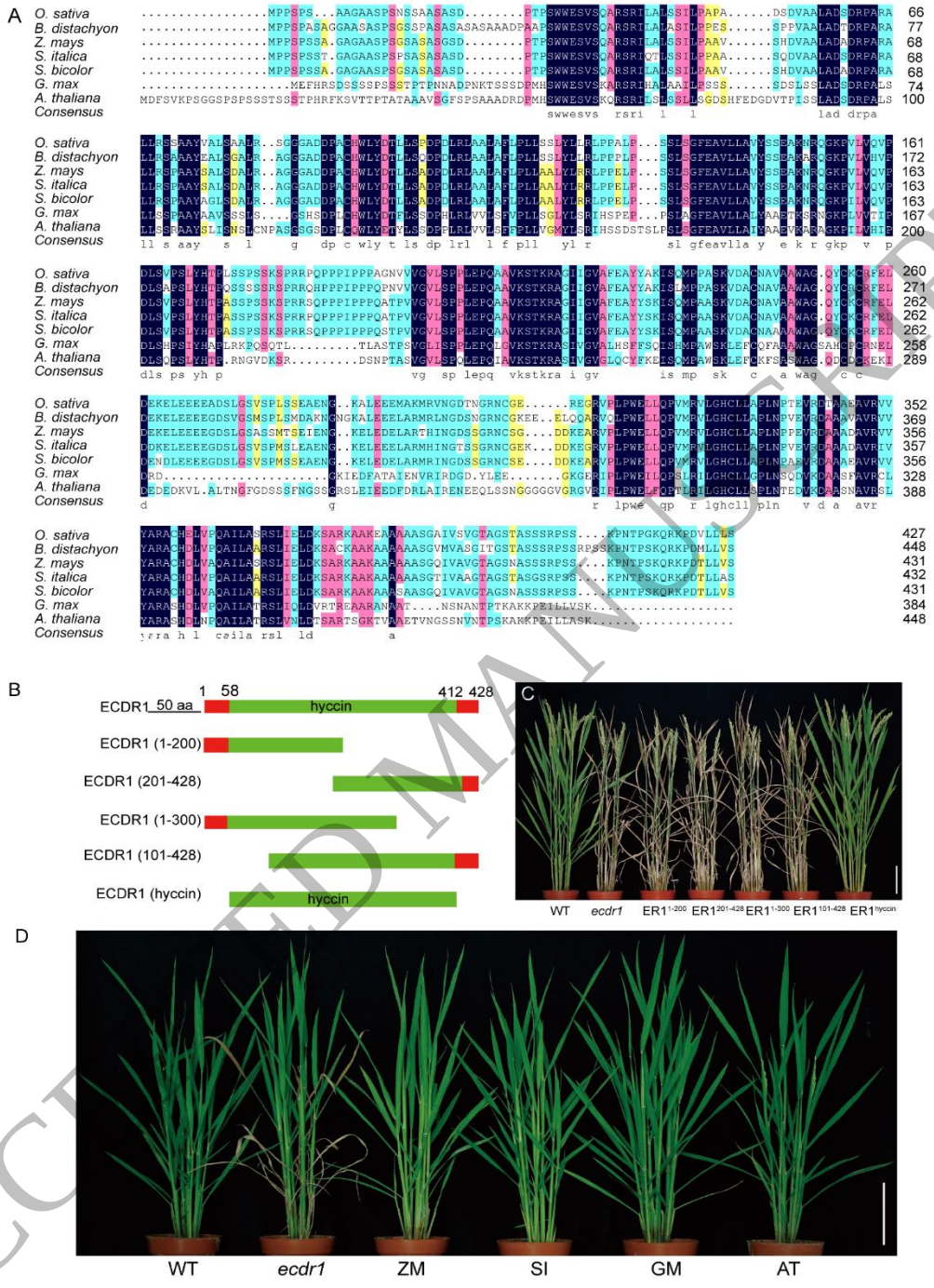

Figure 4
187x259 mm (x DPI)

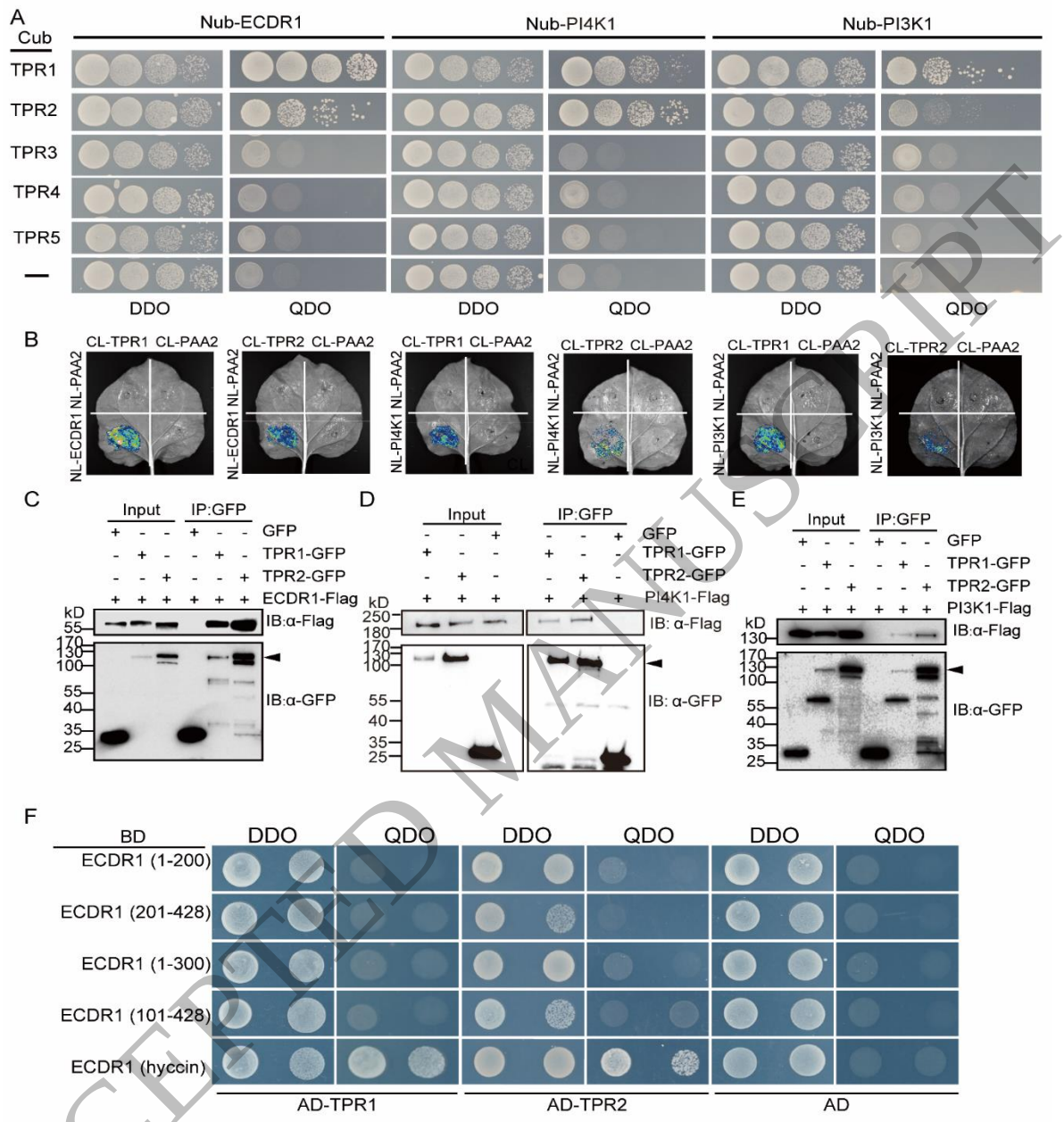

Figure 5
197x228 mm (x DPI)

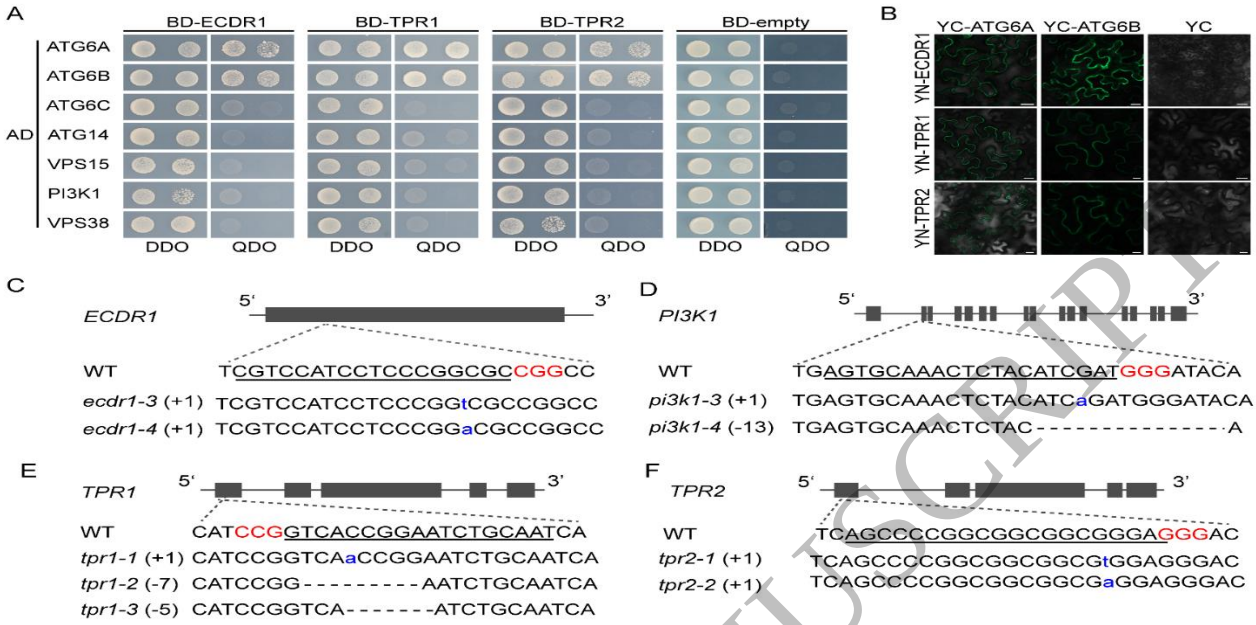

Figure 6
203x144 mm (x DPI)

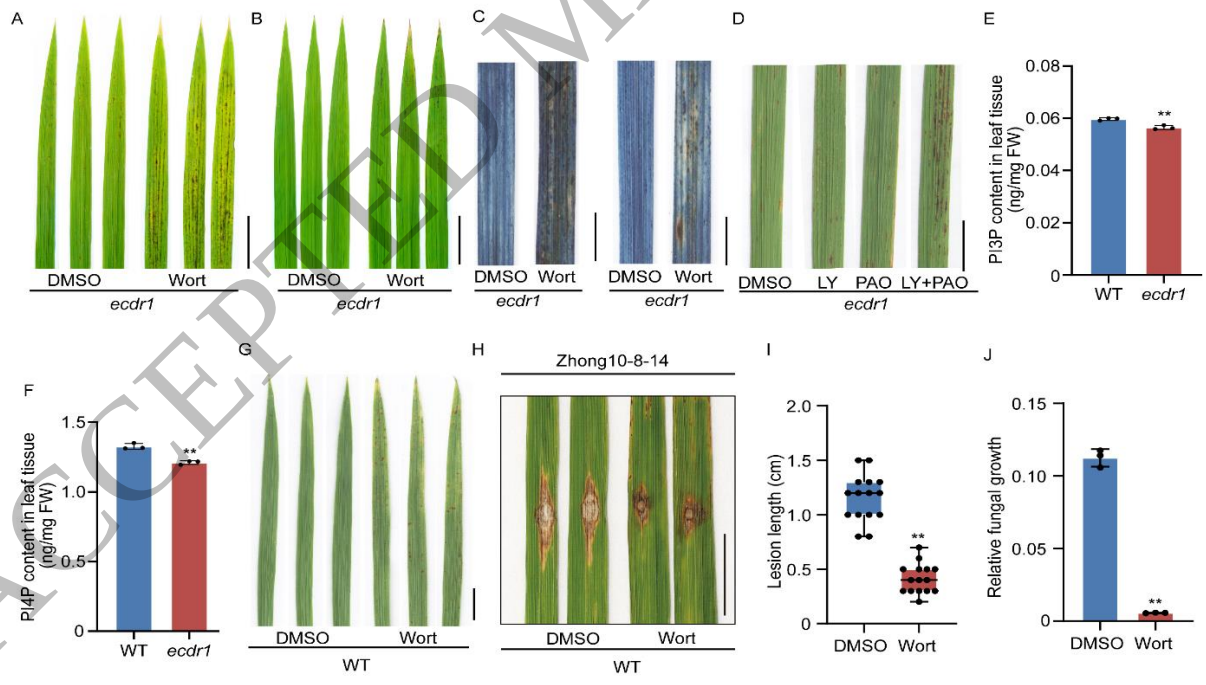

Figure 7
297x181 mm (x DPI)

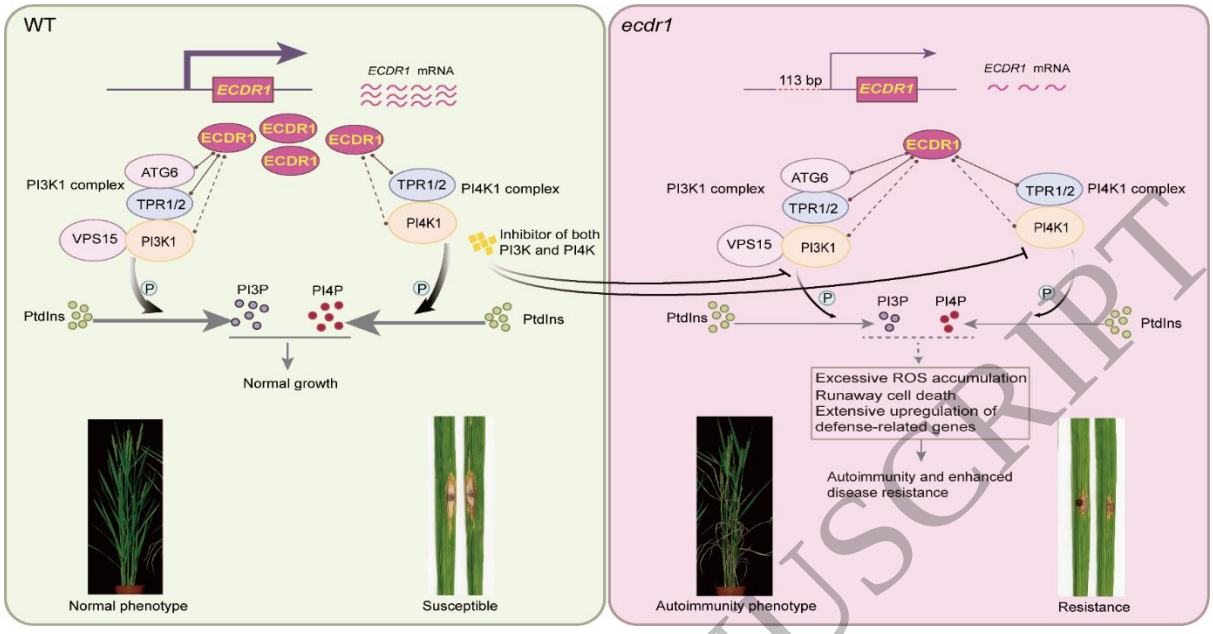

Figure 8
204x117 mm (x DPI)s